JCI insight

Scn2a severe hypomorphic mutation decreases excitatory synaptic input and causes autism-associated behaviors

Hong-Gang Wang, … , Anjali M. Rajadhyaksha, Geoffrey S. Pitt

JCI Insight. 2021. https://doi.org/10.1172/jci.insight.150698.

Research In-Press Preview Neuroscience

Graphical abstract

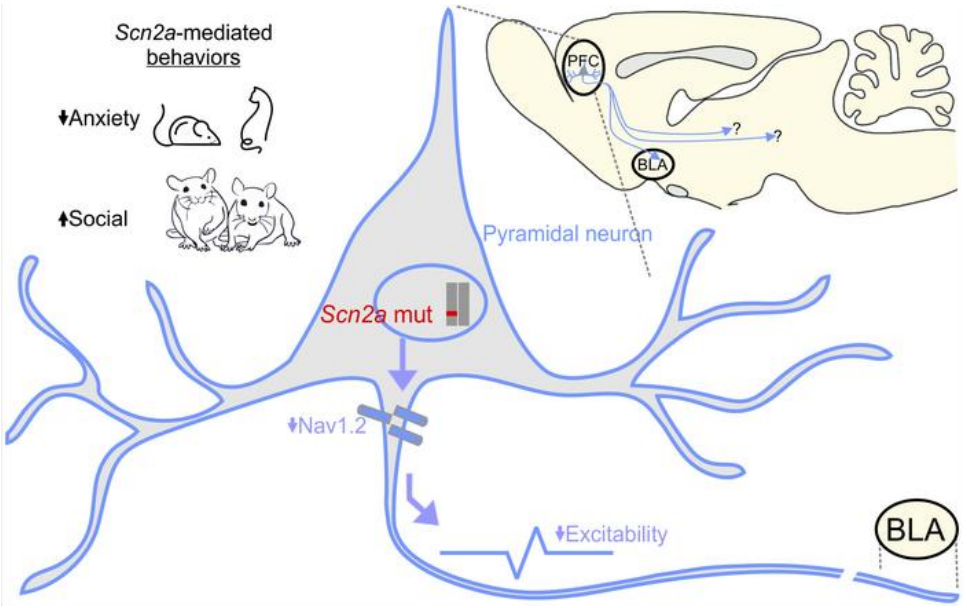

Scn2a severe hypomorphic mutation decreases excitatory synaptic input and causes autism-associated behaviors

Running title: *Scn2a* mouse model shows autism-associated behaviors

Hong-Gang Wang[1], Charlotte C. Bavley[2,3], Anfei Li[2], Rebecca M. Jones[4,5,6], Jonathan Hackett[3], Yared Bayleyen[1], Francis S. Lee[2,5,6], Anjali M. Rajadhyaksha[2,3,5], Geoffrey S. Pitt[1,5]

[1] Cardiovascular Research Institute, Weill Cornell Medicine, New York, NY 10021
[2] Feil Family Brain and Mind Research Institute, Weill Cornell Medicine, New York, NY 10021
[3] Pediatric Neurology, Department of Pediatrics, Weill Cornell Medicine, New York, NY 10021
[4] Weill Cornell Medicine, Center for Autism and the Developing Brain, 21 Bloomingdale Road, White Plains, NY 10305
[5] Weill Cornell Autism Research Program, Weill Cornell Medicine, New York, NY 10021
[6] Sackler Institute for Developmental Psychobiology, Department of Psychiatry, Weill Cornell Medicine, New York, NY

Corresponding author:
Geoffrey S. Pitt
Weill Cornell Medicine
413 East 69th Street
Belfer 502 / Box 190
New York, NY 10021

geoffrey.pitt@med.cornell.edu
Tel: 646-962-7641

ABSTRACT

SCN2A, encoding the neuronal voltage-gated Na^+ channel $Na_V1.2$, is one of the most commonly affected loci linked to autism spectrum disorders (ASDs). Most ASD-associated mutations in *SCN2A* are loss-of-function, but studies examining how such mutations affect neuronal function and whether *Scn2a* mutant mice display ASD endophenotypes have been inconsistent. We generated a protein truncation variant *Scn2a* mouse model (*Scn2a*$^{\Delta 1898/+}$) by CRISPR that eliminates the $Na_V1.2$ channel's distal intracellular C-terminal domain and analyzed the molecular and cellular consequences of this variant in a heterologous expression system, in neuronal culture, in brain slices, and *in vivo*. We also analyzed multiple behaviors in wild type and *Scn2a*$^{\Delta 1898/+}$ mice and correlated behaviors with clinical data obtained in human subjects with *SCN2A* variants. Expression of the $Na_V1.2$ mutant in a heterologous expression system revealed decreased $Na_V1.2$ channel function and cultured pyramidal neurons isolated from *Scn2a*$^{\Delta 1898/+}$ forebrain showed correspondingly reduced voltage-gated Na^+ channel currents without compensation from other central nervous system voltage-gated Na^+ channels. Na^+ currents in inhibitory neurons were unaffected. Consistent with loss of voltage-gated Na^+ channel currents, *Scn2a*$^{\Delta 1898/+}$ pyramidal neurons displayed reduced excitability in forebrain neuronal culture and reduced excitatory synaptic input onto the pyramidal neurons in brain slices. *Scn2a*$^{\Delta 1898/+}$ mice displayed several behavioral abnormalities, including abnormal social interactions that reflect behavior observed in humans with ASD and with harboring loss-of-function *SCN2A* variants. This model and its cellular electrophysiological characterizations provide a framework for tracing how a *SCN2A* loss-of-function variant leads to cellular defects that result in ASD-associated behaviors.

INTRODUCTION

Within the central nervous system (CNS), voltage-gated Na^+ (Na_V) channels such as the *SCN2A*-encoded $Na_V1.2$ initiate action potentials (APs) and are thus fundamental to defining neuronal excitability. In addition to $Na_V1.2$, which is found in excitatory neurons and a small set of inhibitory interneurons (1), the major Na_V channels are *SCN1A*-encoded $Na_V1.1$ (expressed mainly in inhibitory neurons), *SCN3A*-encoded $Na_V1.3$ (expressed in embryonic neurons), and *SCN8A*-encoded $Na_V1.6$ (found in excitatory and inhibitory neurons). Most mature excitatory CNS neurons express $Na_V1.2$ and $Na_V1.6$, and these Na_V channels confer distinct features that tweak electrical activity and contribute to the defining features of AP initiation and conduction in different types of neurons. During early brain development, $Na_V1.2$ is the dominant Na^+ channel expressed in excitatory neurons, where it predominantly localizes to the axon initial segment (2, 3). Because of this preferential expression of $Na_V1.2$ during the vulnerable developmental period when most ASD-associated mutations exert their influence (4), $Na_V1.2$ is well positioned to exert a potent effect on AP initiation and conduction, thereby influencing neuronal excitability and activity-dependent development in the maturing brain.

Next generation sequencing studies of *de novo* mutations in subjects with ASD have consistently identified *SCN2A* as one of the most commonly associated loci (5-7) and *SCN2A* is also among the top loci identified with postzygotic mutations associated with ASD (8). Variants in *SCN2A* have also been linked to several other neurological disorders, including epilepsy and intellectual disability (9). Analyses in heterologous expression systems of several disease-associated *SCN2A* variants found that ASD-associated mutations generally cause channel loss-of-function (often because of protein truncation variants), while epilepsy-associated mutations reveal various biophysical gain-of-function (increased Na^+ influx) effects (10).

Recent examinations of *Scn2a* heterozygous knockout (*Scn2a*$^{+/-}$) mice showed that, in addition to the critical role in the axonal excitability in early development, Nav1.2 is crucial to action potential backpropagation, dendritic excitability, synaptic transmission and synaptic plasticity in mature pyramidal neurons (11, 12). These *Scn2a*$^{+/-}$ mice revealed a decrease in learning and memory (13) but other behavioral consequences, especially those associated with autistic-like behaviors, were highly variable and often inconsistent (11, 12, 14, 15). Therefore, the specific contribution of $Na_V1.2$ dysfunction to ASD endophenotypes has not been determined.

A perturbation of the delicate balance between neuronal excitation and inhibition (E/I balance) has been implicated in a range of neurodevelopmental disorders (4), and a leading hypothesis is that ASD results from an

E/I imbalance in developing circuits during the critical neonatal period (16, 17). Exploiting mice with a Nav1.2 protein truncation variant (*Scn2a*$^{\Delta 1898/+}$) leading to severe reduction in channel function we investigated the consequences on neuronal cellular properties and synaptic transmission to examine effects on E/I balance and ASD-associated behaviors. We found that severe reduction of Nav1.2 function reduced neuronal excitability in cultured forebrain pyramidal neurons isolated from *Scn2a*$^{\Delta 1898/+}$ forebrains, and decreased excitatory synaptic input to pyramidal neurons in the medial frontal cortex (mPFC) and basolateral amygdala (BLA) in acute brain slice from adult *Scn2a*$^{\Delta 1898/+}$ mice. *Scn2a*$^{\Delta 1898/+}$ mice displayed several behavioral abnormalities including enhanced sociability and lack of typical social habituation, consistent with behavior in humans with loss-of-function variants in *SCN2A*. Together, this model and the accompanying cellular electrophysiological characterizations provide a framework for tracing a *SCN2A* loss-of-function variant to cellular and synaptic defects and the resulting altered E/I balance that is associated with ASD-associated behaviors.

RESULTS

Scn2a severe hypomorph mouse model

Like all other Na_V channel α subunits, the *SCN2A*-encoded $Na_V1.2$ has pseudotetrameric repeats of 6 transmembrane segments (**Fig. 1A**) joined by intracellular loops and flanked by cytoplasmic N- and C-termini. The *SCN2A* transcript contains 27 exons, the last of which is the largest and encodes ~ 400 amino acids that include the fourth tetrameric repeat and the C-terminus. In a compendium accompanying a recent study identifying risk genes with autism and developmental-disability biases, seven of 27 *SCN2A* mutations were within this exon (consistent with the length of polypeptide as a fraction of the overall length of the channel), five of which induced a frameshift and protein truncation (7). Overall, 8 of 27 *SCN2A* mutations in that compendium had a frameshift, so frameshifts may be over-represented in this final exon. While generating a single point mutation mouse knockin model of an *SCN2A* disease mutation using CRISPR/Cas9 (to be reported separately), we serendipitously also obtained an indel that produced a frameshift after T1898 in the $Na_V1.2$ C-terminus and a subsequent stop codon following 26 novel amino acids (p.T1898NfsX27) as shown in **Fig. 1A and Supp. Fig 1**. Truncation of $Na_V1.2$ at T1898 eliminates the binding site for the channel auxiliary subunit calmodulin (**Fig. 1A**), which regulates the persistent Na^+ current (18, 19). Because the indel fit a pattern (protein truncation variant in the final exon) common to multiple ASD-associated mutations in *SCN2A*, we chose to analyze the consequences of this allele (*Scn2a*$^{\Delta 1898}$) further.

Heterozygous *Scn2a*$^{\Delta 1898/+}$ mice were viable and fertile, but we never obtained homozygous *Scn2a*$^{\Delta 1898/\Delta 1898}$ mice at weaning from heterozygous crosses (*Scn2a*$^{\Delta 1898/+}$, n=24; wild type (*WT*), n=13; *Scn2a*$^{\Delta 1898/\Delta 1898}$, n=0; χ^2=12.4, p<0.01). Since *Scn2a*$^{-/-}$ display perinatal mortality due to hypoxia from absent respirations (20), we suspect that the *Scn2a*$^{\Delta 1898}$ is a severe hypomorphic allele. The ~2:1 ratio of *WT* to *Scn2a*$^{\Delta 1898/+}$ heterozygotes suggests that *Scn2a* haploinsufficiency does not affect survival, as previously observed (20).

To determine the consequences to $Na_V1.2$ Na^+ currents, we expressed a frameshifted human $Na_V1.2$ channel ($Na_V1.2^{\Delta 1897}$, equivalent to $Na_V1.2^{\Delta 1898}$ in mice) in HEK293 cells and recorded Na^+ currents by whole-cell voltage clamp. Compared to cells expressing $Na_V1.2^{WT}$ channels, cells with $Na_V1.2^{\Delta 1897}$ channels showed markedly decreased Na^+ current density (**Fig. 1B-C**). We also measured currents from a human $Na_V1.2$ in which we inserted a stop codon after T1897 ($Na_V1.2^{1897\text{-}STOP}$), thereby eliminating the alternative 26 amino acids generated by the frame shift, and observed a similar reduction in current density (**Fig. 1C**). In addition to reducing current

density, we found that both the frameshift and the truncation decreased channel availability, as indicated by the leftward shift of the channel steady-state inactivation curves (**Fig. 1D**). The $V_{1/2}$ for steady-state inactivation was –77.9 mV and –74.0 mV for $Na_V1.2^{\Delta 1897}$ and $Na_V1.2^{1897\text{-}STOP}$, respectively, a significant hyperpolarizing shift from the –67.7 mV for the *WT* channel.

To examine whether the reduced Na^+ current resulted from less $Na_V1.2^{\Delta 1897}$ or $Na_V1.2^{1897\text{-}STOP}$ protein inserted into the plasma membrane, we performed surface biotinylation, streptavidin pull down, and quantification of surface $Na_V1.2$ by immunoblot. **Fig. 1E-F** show that, compared to $Na_V1.2^{WT}$, total $Na_V1.2^{\Delta 1897}$ or $Na_V1.2^{1897\text{-}STOP}$ protein was ~40% of $Na_V1.2^{WT}$ and the amount of $Na_V1.2^{\Delta 1897}$ or $Na_V1.2^{1897\text{-}STOP}$ inserted into the plasma membrane was similarly reduced to ~32% of $Na_V1.2^{WT}$. These data suggest that the frameshift/truncation led to decreased protein synthesis or increased degradation, but did not exert significant effects on trafficking to the plasma membrane. Since $Na_V1.2^{1897}$ and $Na_V1.2^{1897\text{-}STOP}$ displayed nearly identical biophysical effects and showed similar degrees of protein instability, we conclude that the additional 26 amino acids generated by the frameshift do not overtly influence $Na_V1.2$ channel function. Thus, $Na_V1.2^{\Delta 1897}$ behaved as a mutant channel with severely reduced function. These heterologous system data suggested that *Scn2a*$^{\Delta 1898/+}$ mice represented an excellent platform to investigate loss-of-function *Scn2a*-associated ASD in an animal model.

To test whether the mutation also led to reduced $Na_V1.2$ protein *in vivo* as observed in HEK293 cells, we analyzed the amount of $Na_V1.2$ protein in lysates from cortex isolated from *Scn2a*$^{\Delta 1898/+}$ mice and their *WT* littermates. We generated lysates from P6 neonates, a stage when $Na_V1.2$ is the dominant voltage-gated Na^+ channel in excitable cells before $Na_V1.6$ replaces most $Na_V1.2$ at the axon initial segment, and separately from adult (~5 month old) animals. In both P6 and adult mice, we observed less $Na_V1.2$ protein in *Scn2a*$^{\Delta 1898/+}$ mice (reduced by ~60%), as detected by two different $Na_V1.2$-specific antibodies targeting distinct epitopes in the channel (**Fig. 2A-B and Supp. Fig. 3**). Using an antibody that recognizes all voltage-gated Na^+ channels, we did not observe a statistically significant reduction in total Na^+ channel protein in cortex lysates from P6 neonatal and adult *Scn2a*$^{\Delta 1898/+}$ mice compared to their respective *WT* littermate controls (**Fig. 2A-B and Supp. Fig. 3**). This is likely because $Na_V1.2$ is just one of the CNS Na^+ channels, and the loss of $Na_V1.2$ from one *Scn2a* allele is insufficient to detect a significant reduction in the total Na^+ channel protein pool.

Truncated proteins are often subjected to rapid degradation. To examine if $Na_V1.2^{\Delta 1898}$ channels were subject to degradation, we stained brain slices from newborn *WT* and *Scn2a*$^{\Delta 1898/\ \Delta 1898}$ mice (which show perinatal

lethality) for $Na_V1.2$. Nav1.2 was abundantly present in the axonal initial segment of *WT* mice, which was labeled with axon initial segment-specific marker ankyrin G, in the layer 2/3 neocortex from *WT* mice, but was almost completely absent in the cortical tissue from *Scn2a*$^{\Delta 1898/\Delta 1898}$ mice (**Fig. 2C**). These data suggest that *Scn2a*$^{\Delta 1898}$ encodes an unstable protein and functions as a severe hypomorphic allele.

Since total Na^+ channel protein in brains from P6 and adult mice was not statistically different between genotypes, we ascertained whether the observed reduction in $Na_V1.2$ protein led to a compensatory upregulation of other Na^+ channel isoforms in the CNS. We performed quantitative real-time polymerase chain reaction RT-qPCR on mRNA isolated from cortex of P3-P6 and adult mice and quantified the relative levels of transcripts for other Na^+ channel isoforms. We did not observe genotype-specific differences between *Scn2a*$^{\Delta 1898/+}$ and *WT* mice in the transcript levels for *Scn1a*, *Scn2a*, *Scn3a*, or *Scn8a* (**Fig. 2D-E**). That there were no genotype-specific differences for *Scn2a* transcripts, specifically, suggests that the reduced $Na_V1.2$ protein in *Scn2a*$^{\Delta 1898/+}$ mice derives from $Na_V1.2^{\Delta 1898}$ protein instability and degradation.

Neuronal cellular consequences of a Scn2a severe hypomorphic allele

Having established the biophysical and biochemical consequences of the severe hypomorphic *Scn2a*$^{\Delta 1898}$ allele, we queried the resulting cellular electrophysiological consequences. To best avoid the voltage clamp challenges of Na^+ currents in brain slice recordings, we characterized the effect of *Scn2a*$^{\Delta 1898/+}$ on neuronal cellular properties in young neuronal cultures, when neurons have less branches and Nav1.2 is the dominantly expressed Na^+ channel. We isolated forebrain neurons from P1-P3 pups, cultured them for 5-7 days, and recorded total voltage-gated Na^+ currents by whole-cell voltage clamp from pyramidal-shaped (excitatory) neurons (**Supp. Fig. 2A**). Peak current density was markedly reduced in neurons from *Scn2a*$^{\Delta 1898/+}$ mice compared to their *WT* littermate controls. The I-V relationships shown in **Fig. 3A** revealed a ~ 38% reduction in Na^+ channel current density in *Scn2a*$^{\Delta 1898/+}$ neurons. If we assume, based on the results in **Fig. 2**, that this reduction represents the almost complete loss of one *Scn2a* allele, we calculate that $Na_V1.2$ contributes ~75% of the total voltage-gated Na^+ channel current in these young cortical pyramidal neurons. Because $Na_V1.2$ has also been found in small set of inhibitory interneurons (1), we also analyzed the I-V relationships of Na^+ currents in non-pyramidal shape neurons (**Supp. Fig. 2B**). As shown in **Fig. 3B**, there was no difference in current density in *Scn2a*$^{\Delta 1898/+}$ vs. *WT* neurons. This is consistent with the reported results (21), showing reduced $Na_V1.2$ currents in excitatory, but not inhibitory neurons. Together, these data further support our interpretation that *Scn2a*$^{\Delta 1898/+}$

mice represent a loss-of-function model.

As *Scn2a* is almost exclusively expressed in excitatory neurons, and since Na^+ channels drive action potentials, we characterized action potentials elicited in the cultured forebrain pyramidal neurons in which we identified the reduction in total Na^+ currents for *Scn2a*$^{\Delta 1898/+}$ mice. We first measured the stimulus threshold at which action potentials were elicited and found that the threshold to elicit APs in cultured *Scn2a*$^{\Delta 1898/+}$ pyramidal cortical neurons was significantly higher than that needed in *WT* neurons (**Fig. 3C**). Moreover, the action potential shape (**Fig. 3D**) and kinetic parameters (**Table 1**) differed. Although our qPCR data (**Fig. 2D-E**) demonstrated the absence of transcriptional compensation from other CNS voltage-gated Na^+ channels, we cannot exclude compensatory changes from other Na^+ channels inserted into specific cellular locations normally dominated by $Na_V1.2$, nor by other, non-Na^+ channel ionic currents that underlie the action potential. We attempted to assess the compensation from non-Na^+ channel ionic currents by analyzing action potentials elicited by a strong stimulus designed to overcome the relative $Na_V1.2$ channel deficit in *Scn2a*$^{\Delta 1898/+}$ neurons. For a stimulus that elicited a maximal amplitude action potential, we no longer observed a difference in the AP amplitude between *Scn2a*$^{\Delta 1898/+}$ and *WT* littermate control neurons, suggesting that the reduced AP amplitude in *Scn2a*$^{\Delta 1898/+}$ neurons derived mainly from the reduced Na^+ current amplitude (**Fig. 3E** and **Table 2**). Further, we observed a marked decrease in the number of spikes elicited from *Scn2a*$^{\Delta 1898/+}$ neurons across a range of stimulation intensities and, consistent with the reduced overall Na^+ channel current amplitude in *Scn2a*$^{\Delta 1898/+}$ neurons, the latency to first spike was longer than in *WT* neurons (**Fig. 3F-H**). Together, these data showed that the *Scn2a*$^{\Delta 1898/+}$ pyramidal neurons were less excitable than *WT* neurons.

Behavioral consequences of a Scn2a severe hypomorphic allele

Having established a $Na_V1.2$ loss-of-function defect in *Scn2a*$^{\Delta 1898/+}$ forebrain neurons, we investigated whether this mutation conferred consequences on behavior. We first assessed general locomotor activity in a novel environment open field arena. Mutants of both sexes showed no deficits in locomotion, but rather increased locomotion compared to *WT* mice (**Fig. 4A**). We then assessed core ASD-associated behaviors, repetitive behavior and social interaction. Using grooming time as a correlate of repetitive behaviors (22), we observed no genotype-specific differences in either males or females (**Fig. 4B**). We then assayed sociability in a 5-minute three-chamber social interaction test. Both male and female *WT* controls and *Scn2a*$^{\Delta 1898/+}$ mice spent more time with a novel mouse than with a novel object (**Fig. 4C-D**). However, male *Scn2a*$^{\Delta 1898/+}$ mice spent more time with

the novel mouse compared to their *WT* controls (**Fig. 4D**). This was also reflected in higher distance traveled by *Scn2a*$^{\Delta 1898/+}$ compared to *WT* mice in the zone around the novel mouse (**Supp. Fig. 4A**), with no difference in distance traveled around the object (**Supp. Fig. 4A**) and other areas of the 3 chamber apparatus (**Supp. Fig. B-C**). To further explore this effect we utilized a modified three chamber social interaction protocol to monitor sociability and habituation to a novel mouse, typically seen in *WT* mice across repeated testing sessions (23, 24). A separate cohort of male *Scn2a*$^{\Delta 1898/+}$ and *WT* mice underwent an initial three-chamber social interaction test (the first test) followed by an additional test, at 3 hours (same stranger) after the first test. As we observed above (**Fig. 4C-D**), both *WT* controls and *Scn2a*$^{\Delta 1898/+}$ mice showed a social preference during the first test. During the subsequent test, the *WT* controls showed the expected habituation to the familiar mouse (3 hours after) (23), in contrast, the *Scn2a*$^{\Delta 1898/+}$ mice continued to spend significantly more time with the familiar mouse during the subsequent test (**Fig. 4E**). These data support that *Scn2a*$^{\Delta 1898/+}$ mice display altered social interaction behavior characterized by sustained time with the social stimulus. Interestingly, human ASD subjects with *SCN2A* mutations were reported to "enjoy physical contact with caregivers" (25). Further, clinical data from the Simons Variation in Individuals Project (VIP) data (v. 3.0) for individuals with *SCN2A* variants whose caregiver completed the Autism Diagnostic Interview-Revised (ADI-R) (26) with a clinician support those observations. In this largest publicly available database of clinical data in patients with *SCN2A* variants, ten individuals had an *SCN2A* variant and ADI-R data, seven who were classified as having autism from the Autism Diagnostic Observation Schedule (ADOS) (27), two as non-spectrum, and one with missing data. Four of the ten individuals had a protein truncation variant with a frameshift. The ADI-R includes a question "*Social Disinhibition*" that queries whether the child exhibits behavior that is not appropriately modulated according to the social situation, such as inappropriately friendly (*i.e.*, approaching or touching strangers), or if the child is more socially naive than other children (*i.e.*, unable to understand what to say or do in a particular social situation). Caregiver answers were scored on a four-point scale. Three children scored "occasional disinhibition"; 5 scored "lack of social inhibition"; and 2 scored "marked social disinhibition." None reported an absence of disinhibition. Thus, the social interaction abnormality displayed by *Scn2a*$^{\Delta 1898/+}$ mice correlates well with observations of humans with *SCN2A* variants and with the inappropriate social disinhibition observed in individuals with *SCN2A* mutations.

Inappropriate social contact with strangers, often characterized as overfriendliness, is a feature of Williams syndrome (WS), a neurodevelopmental disorder caused by hemizygous deletion of 7q11.23 (ref. (28)). A mouse model of WS shows increased social interaction and lack of habituation to a stranger mouse (29), suggestive of the phenotype we observed in the *Scn2a*$^{\Delta 1898/+}$ mice. While the underlying genetic defect in subjects with WS is distinct from the loss-of-function mutations in *SCN2A*-associated ASD subjects, we considered the possibility that the underlying circuit level deficits in WS provided guideposts to uncover circuit deficits in ASD subjects with *SCN2A* mutations. A recent review (30) attributed the increased social interaction phenotype in WS subjects to impaired detection of danger, therefore motivating us to test for impaired danger detection in *Scn2a*$^{\Delta 1898/+}$ mice. We examined performance on an elevated plus maze (EPM) that assesses innate fear and anxiety (31). Both male and female *Scn2a*$^{\Delta 1898/+}$ mice spent more time, and traveled longer distances, in the open arms than their *WT* littermate controls (**Fig. 5A-C**). Neither sex displayed any difference in number of entries to the open arms or closed arms, and there was no difference in time spent and distance traveled in the closed arms (**Fig. 5B-D**). Therefore, the genotype-specific differences are restricted to the open arms, so the EPM data suggest decreased anxiety-like behavior.

Neuronal synaptic transmission consequences of a Scn2a severe hypomorphic allele

Both mPFC and amygdala are central hubs integrating distinct functional signals related to higher cognitive and emotional behaviors including sociability and fear (32-34). Since *Scn2a*$^{\Delta 1898/+}$ mice display abnormal social interaction and decreased fear-like behavior, we next tested the influence of the decreased neuronal excitability of *Scn2a*$^{\Delta 1898/+}$ on synaptic properties and on the E/I balance in brain slices with inclusion of mPFC or BLA from adult mice. We measured spontaneous excitatory and inhibitory postsynaptic currents (sEPSCs and sIPSCs) in pyramidal neurons in layer 5/6 of the mPFC and in the BLA (**Supp. 5A-B**). The frequency of sEPSCs was reduced in *Scn2a*$^{\Delta 1898/+}$ mice compared to *WT* littermate controls in both mPFC and BLA pyramidal neurons, suggesting reduced excitatory synaptic input (**Fig. 6A-B, and 6D**). The average sIPSC frequency trended towards a decrease but did not reach statistical difference (**Fig. 6A, 6C and 6E**). On the other hand, sEPSC and sIPSC amplitudes were comparable between *WT* and *Scn2a*$^{\Delta 1898/+}$ mice (**Fig. 6A-E**), suggesting no postsynaptic differences between genotypes. These data, combined with the observed effects on elicited APs and excitability in pyramidal neurons, the observed lack of an effect on Na^+ currents in inhibitory neurons, and the reported

absence of a change in inhibitory neuron excitability (21) suggest that neuronal firing was reduced in *Scn2a*$^{\Delta 1898/+}$ pyramidal neurons, leading to a reduction in excitatory input to postsynaptic neurons. Overall, this suggests a decrease in excitatory synaptic transmission in *Scn2a*$^{\Delta 1898/+}$ neurons.

In vivo neuronal activity consequences of a Scn2a severe hypomorphic allele

We next examined whether the decreased excitability measured in cultured neurons and the decreased synaptic transmission in slices correlated with decreased activity *in vivo* and with consequences on behavior. We injected a virus encoding the neuronal activity sensor GCaMP6s into mPFC, as circuits from the amygdala to the mPFC have been implicated in fear (35), and tested calcium dynamics in GCaMP6s expressing neurons with fiber photometry during EPM (**Fig. 6F**). When traveling into an open arm on the EPM, *WT* mice showed an increase in neuronal activity starting within 1 second of open arm entry, but no increase when entering a closed arm. In contrast, *Scn2a*$^{\Delta 1898/+}$ mice displayed no increase in activity when entering either the open or closed arm (**Fig. 6G**). This result echoes the decreased neuronal activity observed in the *Scn2a*$^{\Delta 1898/+}$ mice in the cellular and slice recordings and provides a correlation between abnormal neuronal activity and abnormal behavior in *Scn2a*$^{\Delta 1898/+}$ mice.

DISCUSSION

Although next generation sequencing showed that *de novo* loss-of-function protein truncation variants in *SCN2A*, often associated with a frameshift, are among the most common genetic associations with ASD (7, 8), the mechanisms leading to ASD-associated endophenotypes have not been definitively determined. Here, we demonstrated that an *Scn2a* protein truncation variant that appears to be rapidly degraded reduced the number of functional channels and the amount of voltage-gated Na^+ current in excitatory neurons in which *Scn2a* is predominantly expressed. Consistent with reduced $Na_V1.2$, we found that *Scn2a*$^{\Delta 1898/+}$ pyramidal neurons were less excitable. Our observations in mouse neurons, slices, and *in vivo* echo a report in which knockout of *SCN2A* in neurons derived from induced pluripotent stem cells reduced extracellular spontaneous network activity in glutamatergic neurons (36).

Moreover, our analyses reveal correlations between the cellular abnormalities and changes in behavior in *Scn2a*$^{\Delta 1898/+}$ mice that, to date, have been elusive when considering the various reported studies of *Scn2a*$^{+/-}$ models. Those studies (11, 12, 14, 15) have shown marked discrepancies in the autistic-like and other ASD comorbid behavior phenotypes. For instance, some studies reported increased social interaction (12, 14), while others reported a mild decrease (11, 15); some studies reported increased grooming in a novel environment (14, 15), while another failed to detect abnormal grooming (12). The reasons for the discrepant results despite using identical or nearly identical models is not clear. Thus, the utility of comparing a different *Scn2a* haploinsufficient model provides an opportunity to define which endophenotypes most likely result from reduced $Na_V1.2$ expression.

While we cannot completely rule out a contribution of the additional 26 amino acids generated by the frameshift in the *Scn2a*$^{\Delta 1898/+}$ mice, our data suggest that the additional 26 amino acids have no discernible effect on $Na_V1.2$ channel function: a $Na_V1.2$ protein with a stop codon inserted at T1898 displayed identical channel properties, as shown in **Fig. 1**. Moreover, the truncated and frameshifted $Na_V1.2$ behaves *in vivo* like a severe hypomorphic allele, as suggested by several lines of evidence. First, the complete absence of surviving *Scn2a*$^{\Delta 1898/\Delta 1898}$ pups is consistent with the perinatal lethality of *Scn2a*$^{-/-}$ mice (20). Secondly, our biochemical and electrophysiological analyses suggest little, if any, functional protein from the mutant allele (**Fig. 2 and Fig. 3**). Therefore, by demonstrating functionally equivalent biophysical and biochemical consequences of the truncation and the frameshift variant in a heterologous expression system, our data show that the reduced Na^+

channel function recorded in neurons isolated from *Scn2a*$^{\Delta 1898/+}$ mice result from the eliminated $Na_V1.2$ protein rather than the introduction of the additional 26 amino acids. Thus, the hypomorphic *Scn2a*$^{\Delta 1898/+}$ model is representative of ASD-associated mutations in *SCN2A*, such as D82G or T1420M (10).

With that background, the *Scn2a*$^{\Delta 1898/+}$ mice displayed an increase in social interaction [consistent with (12, 14)]; and an increase in locomotor activity, along with reduced anxiety-like behavior [consistent with (11, 14, 15)]. We also observed no change in grooming in *Scn2a*$^{\Delta 1898/+}$ mice, consistent with the previous report by Shin et al. (12). Thus, the overlaps with our distinct model suggests validation for those behavior abnormalities as indeed associated with *Scn2a* haploinsufficiency. Additionally, the hyper-social interaction phenotype, reported by several groups using a three-chamber social interaction test for various mouse models (14, 29, 37-40) and specifically in the *Scn2a*$^{+/-}$ model (12, 14) appears to be consistent with the inappropriate social approach behavior, i.e., inappropriate social disinhibition, reported in individuals with *SCN2A* variants seen in our analysis of the Simons VIP database. Further, our fiber photometry data suggest a direct link from cellular electrophysiology and a specific behavior in the mouse model.

Having established social disinhibition and decreased anxiety (on the EPM) as phenotypes associated with decreased *Scn2a* expression, analysis of circuit deficits in WS may serve a guide for future studies to investigate the consequences of *Scn2a* haploinsufficiency. Functional MRI in individuals with WS showed reduced functional connectivity between the amygdala and the medial prefrontal and orbitofrontal cortex, which was correlated with social disinhibition (41). Recent studies demonstrated that the medial prefrontal cortex makes excitatory projections to principal neurons in the basolateral amygdala (e.g., ref. (42, 43)). We therefore hypothesize that the loss-of-function defects observed in Na^+ currents within pyramidal neurons from *Scn2a*$^{\Delta 1898/+}$ mice, and the consequent reduced excitatory input, impair the excitatory connections from the medial prefrontal to the basolateral amygdala. This, in turn, would reduce amygdala output. The abnormal behavior was correlated to a reduced neuronal activity in mPFC in fiber photometry recording in *Scn2a*$^{\Delta 1898/+}$ mice. Consistent with this hypothesized reduced amygdala output, the *Scn2a*$^{\Delta 1898/+}$ mice demonstrated an impairment in danger detection as observed on the EPM. The similarities among the social disinhibition in humans with *SCN2A* variants, the reported enjoyment of interactions with caregivers for humans with *SCN2A* variants, and the observed social phenotypic abnormality in the *Scn2a*$^{\Delta 1898/+}$ mouse model, suggest a testable cellular to endophenotype connection for future studies. Future circuit level analyses will allow us to test this hypothesis in detail, but the

data here suggest that a neocortical E/I imbalance, whether an increased or decreased ratio, is a substrate for ASD-associated endophenotypes. It is possible that the heterogeneous changes in E/I imbalance (higher or lower) and the consequent alteration in brain network in the temporal and spatial scales could be associated with different manifestations of behavior, which is reflected by the clinical heterogeneity of autistic patients.

While decreased excitability in the principal neurons expressing *Scn2a* with decreased frequency of sEPSCs provides a rationale for that proposed deficit in the prefrontal cortex to amygdala circuit, additional factors may also contribute. We did not observe a significant difference in frequency of sIPSCs between *WT* and *Scn2a*$^{\Delta 1898/+}$ mice, nor a difference in Na^+ currents within inhibitory neurons, although the average frequency of sIPSCs trended to a decrease. The subtle reduction in sIPSCs could represent a homeostatic response aimed to maintain the proper balance between excitation and inhibition through local synaptic adaptions and network-wide adjustments (44), but this change in inhibitory input could not restore the overall deficit in excitatory activity of pyramidal neurons.

We found that the difference in the AP amplitude between *Scn2a*$^{\Delta 1898/+}$ and *WT* littermate control neurons was no longer observed with a stimulus that elicited a maximal action potential amplitude, suggesting that the reduced AP amplitude with a smaller stimulus derived mainly from the reduced Na^+ current amplitude. However, the higher intensity stimulus did not correct the AP threshold, suggesting that the observed differences in action potential between *WT* and *Scn2a*$^{\Delta 1898/+}$ (**Fig. 3E** and **Table 2**) also reflected compensation by other non-Na^+ channel ionic currents. Likely, other homeostatic mechanisms, at the cellular and circuit level, are activated even though those mechanisms appear insufficient to rescue the hyper-social behavior or the decreased anxiety-like behavior and/or impairment of danger detection as indicated by the EPM.

Excitatory neurons within the cortex express both $Na_V1.2$ and $Na_V1.6$, yet mutations in *SCN8A* that encodes $Na_V1.6$ have not been associated with ASD. That expression of $Na_V1.6$ is not prominent until later developmental stages, when critical neural circuits are already established, provides at least one likely reason why *SCN8A* mutations have not been associated with ASD. Consistent with a later role in development for $Na_V1.6$, we did not observe a compensatory increase in *Scn8a* mRNA, or any other CNS Na^+ channel, in the P6 and adult *Scn2a*$^{\Delta 1898/+}$ mice. This absent compensatory response to a reduction in $Na_V1.2$ protein and $Na_V1.2$-dependent Na^+ current in the *Scn2a*$^{\Delta 1898/+}$ mice may offer an additional explanation for why loss-of-function *SCN2A* mutations have been identified as one of the most common genetic associations with ASD.

In summary, the cellular electrophysiology data and the behavior data displayed by the *Scn2a*$^{\Delta 1898/+}$ mice, and the resulting protein truncation variant $Na_V1.2^{\Delta 1898}$, provide valuable tools to investigate the molecular mechanisms by which *SCN2A* mutations cause abnormal social behaviors and offer opportunities to explore therapeutic options for one of the most commonly affected ASD-associated loci.

METHODS

Animals. Animals were handled according to National Institutes of Health Guide for the Care and Use of Laboratory Animals.

Frameshift generation. The *Scn2a*$^{\Delta 1898/+}$ mouse line with a frame shift (p.T1898NfsX27) in one allele of *Scn2a* (**Fig. 1A**) was created by CRISPR/Cas9 by the Transgenic Mouse Shared Resource at Duke University School of Medicine during an attempt to create a *Scn2a*^{R1903C} knockin mutation. The guide sequence (5' GATAGCGTCTGTAAGCTCGCTGG 3') was identified using the online tool at http://crispr.mit.edu/. The guide and repair oligonucleotide (5'-GCTCTTCGAATCCAGATGGAAGAGCGGTTCATGGCTTCCAATCCCTCCAAGGTCTCTTATGAGCCCATTACCACCACTCTGAAG**T**GCAAACAAGAGGAGGTGTCTGCTATTGTCAT**A**CAGCGAGCTTACAGACGCTATCTTCTGAAACAGAAAGTTAAGAAGGTTTCGTCTATATATAAAAAAGACAAGGGTAAAGAAGA-3'; the underlined "T" introduces a C>T point mutation, and the underlined "A" disrupts the PAM sequence and creates a silent mutation within the coding region) were synthesized at Integrated DNA Technologies, Inc. (Coralville, Iowa) and subcloned into pX330 using standard cloning procedures, and produced from recombinant pX330 plasmid using MEGAshortscript™ (Ambion, Foster City, California) following the manufacturer's protocol. sgRNAs were tested *in vitro* using Guide-it™ sgRNA Screening System (Clontech Laboratories, Mountain View, California) following the manufacturer's protocol. The reagents were injected into B6SJLF1/J oocytes to obtain pups that were sequenced by sequencing genomic DNA by PCR. A line with the off-target p.T1898NfsX27 (**Supp. Fig.1**) in one allele was selected for further study.

Heterologous expression system analyses of voltage-gated currents and biotinylation. QuikChange Site-Directed Mutagenesis kit (Agilent Technologies) was used to generate p.T1897NfsX27 ($Na_V1.2^{\Delta 1897}$, equivalent to mouse p.T1898NfsX27) in a human *SCN2A* cDNA subcloned into pCI-Neo. The truncation mutant ($Na_V1.2^{1897\text{-}STOP}$) was also generated with QuikChange, by inserting a stop codon after T1897 in the *SCN2A* cDNA.

Biotinylation analysis. HEK293 cells were cultured in Dulbecco's modified Eagle's culture media with 10% fetal bovine serum in a 37°C incubator with 5% CO_2 and were grown in 100-mm culture dishes. Plasmids encoding wild type $Na_V1.2$ ($Na_V1.2^{WT}$), $Na_V1.2^{\Delta 1897}$, $Na_V1.2^{1897\text{-}STOP}$, or empty vector (8 µg) were co-transfected with *Scn1b* (4 µg) using Lipofectamine 2000 (ThermoFisher Scientific). Forty-eight hours after transfection,

cultured HEK293 cells were washed with ice cold PBS and incubated in 1 mg/ml sulfo-NHS-SS-Biotin (ThermoFisher Scientific) in PBS for 30 minutes at 4°C. Cells were washed twice with 100 mM glycine to quench the reaction, and then were lysed in lysis buffer (NaCl 150 mM, Tris 50 mM, Triton 1% and Roche protease inhibitor 1 tablet/7.5 ml, pH 7.4). After rocking for 30 minutes at 4°C, lysates were passed through 18g and then 25g needles for 25 passes each, then spun at 17,000 x g for 15 minutes at 4°C. Supernatants were collected and protein concentration was quantified using a BCA Protein Assay Kit (ThermoFisher Scientific). Supernatants were incubated and rocked with NeutrAvidin agarose resin (ThermoFisher Scientific) overnight at 4°C. The following day, the beads were washed three times with lysis buffer, resuspended in LDS sample buffer (ThermoFisher Scientific) containing 50 mM DTT and heated to 95°C for 3 minutes. About 20 g of protein were dissolved with LDS sample buffer and separated on Novex™ WedgeWell™ 8–16% Tris–glycine gels (ThermoFisher Scientific) and transferred to PVDF blotting membrane (GE Healthcare Life Sciences). The membrane was immunoblotted with an anti-pan sodium channel antibody (1:1000; Sigma, S8809), anti-transferrin receptor (1:1000; ThermoFisher Scientific, 13-6800) and anti-β-actin (1:5000; Sigma, A1978) antibodies and detected by chemiluminescence. Images were captured using Kodak Image Station 4000 R and quantified using Image J (NIH).

Immunoblotting of brain cortex. About 80 mg neonatal (P6) and adult (~ 5 month old) brain cortices were homogenized with glass homogenizer in RIPA Buffer (ThermoFisher Scientific) containing NaCl 150 mM, Tris-HCl 25 mM, NP-40 1%, sodium deoxycholate 1%, SDS 0.1%, ThermoHalt protease inhibitor and Halt phosphatase inhibitor, pH 7.6. After rocking for 2 hours at 4°C, lysates were passed through 18G and then 25G needles for 25 passes each, then spun at 17,000 x g for 15 minutes at 4°C. Supernatants were collected and protein concentration was quantified using a BCA Protein Assay Kit (ThermoFisher Scientific). Protein 30 g was separated on Novex™ WedgeWell™ 8–16% Tris–glycine gels (Thermo Scientific) and transferred to PVDF blotting membrane (GE Healthcare Life Sciences). The membrane was immunoblotted with anti-pan sodium channel antibody (1:1000; Sigma, S8809), anti-$Na_v1.2$ sodium channel (1:200; NeuroMab, 75-024 and Alomone Labs, ASC-002) and β-actin (1:5000; Sigma, A1978) antibodies. The blots were visualized by chemiluminescence and images were captured using ChemiDocTM Touch Imaging System (Bio-Rad) and quantified using Image J (NIH).

Immunohistochemistry of brain cortex. Brains were rapidly removed from newborn pups and immersed in 0.5% paraformaldehyde in 0.1M phospho-buffer saline (PBS) for 2 hours at 4°C followed by an overnight immersion in 30% sucrose in PBS. Then, brains were embedded in optical cutting temperature compound (OCT) and stored at -80°C overnight. Brain tissue was sectioned to 10-micron slices using a cryostat, and slices were stored overnight in -20°C. Brain sections were thawed for 5 minutes in room temperature, rinsed with 0.1M PBS and incubated with primary antibodies: a custom rabbit Nav1.2 (1:500) designed by YenZym LLC and mouse ankyrin-G (1:200; NeuroMab, N106/36) in PBS with 5% bovine albumin serum and 0.3% triton X-100 overnight at 4°C. Subsequently, after slices were rinsed with 0.1M PBS 3 times each for 5 minutes, the slices were incubated with secondary antibodies Alexa-488 anti-rabbit and Alexa 647 anti-mouse IgG (1:500) at room temperature (25°C) for 1 hour. Slides were then washed with 0.1M PBS for 3 times each for 5 minutes and were mounted using mounting media (Vector laboratories) and sealed with glass cover slip. Slides were kept at 4°C for 2 hours. Stained brain slices were imaged using a confocal microscope (Zeiss LSM 880) and z-stacks were obtained with 0.5um per slice. Images were merged and analyzed using Image-J software.

Quantitative real-time polymerase chain reaction (RT-qPCR). Total mRNA was purified from neonatal (3-6 days) and adult (~ 5 month old) brain cortices using RNAeasy Plus Mini kit (Qiagen, CA), and reverse transcribed to single-stranded cDNA library using iScript cDNA Synthesis Kit (Bio-Rad). Primers for qPCR were 5'-CACTCATTATTCAGCATGTTAATCATGTGC (forward) and 5'-CGATGGTCTTCAGGCCTGGAATG (reverse) for *Scn1a*; 5'-CCAGACTGGACAAAGAATGTGGAGTATAC (forward) and 5'-CGATGGTCTTCAGGCCTGGAAT (reverse) for *Scn2a*; 5'-CCTGACTGGACGAAGAATGTAGAGTACAC (forward) and 5'-CGATGGTCTTTAAACCTGGAATGACTG (reverse) for *Scn3a*; 5'-CATTCAGTCTTCAGCATGATCATCATGTG (forward) and 5'-CGATTGTCTTCAGGCCTGGGAT (reverse) for *Scn8a*; 5'-CCTGGAGAAACCTGCCAAGTATGATG (forward) and 5'-CTGTAGCCGTATTCATTGTCATACCAGG (reverse) for GAPDH. qPCR (a total 40 cycles) was performed using the QuantStudio 3 (Applied Biosystems). The relative amount of target message in each reaction was determined from the detection threshold cycle number (Ct), which was normalized to the Ct for GAPDH obtained simultaneously.

Forebrain cortex neuron cultures. Forebrain cortices from 1- to 3-day newborn *WT* and p.T1898NfsX27 (*Scn2a*$^{\Delta 1898/+}$) mice were dissociated through enzymatic treatment with 0.25% trypsin and subsequent trituration. The cells were plated on glass coverslips previously coated with poly-D-lysine and laminin in 12-well cell culture

plate in the density of 170,000/ml. The cortical cells were grown in neurobasal A medium (ThermoFisher Scientific) supplemented with B-27 2%, glutamine 2 mM, heat-inactivated fetal bovine serum 10% and penicillin/streptomycin 1% in 5% CO_2 incubator at 37º C overnight and then this medium was replaced by one containing B-27 2%, glutamine 0.5 mM, heat-inactivated fetal bovine serum 1%, uridine 70 µM and 5-fluorodeoxyuridine 25 µM. Cultured neurons were used for electrophysiology 5 days (DIV, *days in vitro*) after plating, and recordings were performed on either pyramidal- or non-pyramidal shaped neurons selected based on the shape of their cell body and dendritic pattern (see **Supp. Fig. 2A-B**).

Acute slice preparation. Coronal brain slices were prepared from male and female *Scn2a*$^{\Delta 1898/+}$ mice and their respective littermates (8-10 weeks old). Animals were anesthetized with 1.25% Avertin (250 mg/kg; i.p.) and then transcardially perfused with a cold sucrose-based solution. This solution contained (in mM): sucrose 220, KCl 2.5, $MgSO_4$ 12, $CaCl_2$ 0.5, NaH_2PO_4 1.25, $NaHCO_3$ 26, glucose 10, HEPES 10, and sodium pyruvate 3, pH 7.4. After decapitation, the brain was transferred quickly into the above-mentioned ice-cold sucrose based cutting solution bubbled with 95% O2 and 5% CO2. Coronal brain slices (300 µm) including mPFC or BLA were prepared using a Leica VT1200S vibratome (Leica, Inc), and were incubated in a BSK-2 brain slice keeper (Automate Scientific, CA) containing oxygenated artificial cerebrospinal fluid (aCSF) at 35 °C for 40 min. Afterwards, the slices were maintained at room temperature at least 30 min before use.

Electrophysiology. Whole-cell sodium (Na^+) currents from HEK293 cells and cultured neurons, and spontaneous excitatory (sEPSC) and inhibitory (sIPSC) synaptic currents from acute brain slices were recorded in the voltage patch-clamp configuration, and action potentials (APs) from cultured neurons were recorded in the current-clamp configuration with an Axopatch 200B amplifier (Molecular Devices) and sampled at 10 kHz and filtered at 2 kHz. Data were analyzed with Axon Clampfit (Molecular Devices) or Mini Analysis (Synaptosoft Inc.).

For Na^+ currents recording in HEK cells, the pipette internal solution contained the following (in mM): CsCl 16, CsF 110, NaCl 10, $CaCl_2$ 0.5, $MgCl_2$ 1, EGTA 10, HEPES 10, Na_2-APT 2, pH 7.3 with CsOH; the external solution contained (in mM): NaCl 120, KCl 5.4, $CaCl_2$ 1.8, $MgCl_2$ 1, HEPES 10, glucose 10, tetraethylammonium chloride (TEA-Cl) 20, pH 7.4 with NaOH. For Na+ currents recording in cultured neurons, the pipette internal solution contained (in mM): CsCl 50, CsF 35, L-aspartic acid 55, NaCl 10, EGTA 5, $MgCl_2$ 1, Mg-ATP 4, Na_2-GTP 0.4, HEPES 10, pH 7.3 with CsOH; external solution contained (in mM): NaCl 100, KCl 5, HEPES 20, $CaCl_2$

2, $MgCl_2$ 2, glucose 30, TEA-Cl 20, 4-aminopyridine 2, $CdCl_2$ 0.5, APV 0.05, DNQX 0.02, bicuculline 0.02, pH 7.4 with NaOH. For AP initiation in cultured neurons, the pipette internal solution contained (in mM): potassium gluconate 130, KCl 10, $MgCl_2$ 5, EGTA 0.6, HEPES 5, $CaCl_2$ 0.06, phosphocreatine disodium 10, Mg-ATP 2, Na_2-GTP 0.2, and creatine phosphokinase 50 U/ml, pH 7.2 adjusted with KOH; the external solution contained (in mM): NaCl 119, KCl 5, HEPES 20, $CaCl_2$ 2, $MgCl_2$ 2, glucose 30, APV 0.05, DNQX 0.02, bicuculline 0.02, pH 7.3 adjusted with NaOH. For sEPSCs and sIEPSCs recording from brain slices, the pipette internal contained (in mM): potassium gluconate 125, KCl 10, $MgCl_2$ 5, EGTA 0.6, HEPES 5, $CaCl_2$ 0.06, phosphocreatine disodium 10, Mg-ATP 2, Na_2-GTP 0.2, creatine phosphokinase 50 U/ml and lidocanine N-ethyl bromide 5, pH 7.2 adjusted with KOH; the aCSF containing (in mM); NaCl 126, KCl 2.5, $NaH2PO_4$ 1.25, $NaHCO_3$ 26, $CaCl_2$ 2, $MgCl_2$ 2 and glucose 10. Equilibrium voltage across sEPSCs and sIPSCs recording solutions for Cl^- (E_{Cl}) and cation ions (E_{cation}) were -51 mV and 0 mV, respectively.

For recording Na^+ currents in HEK293 cells, cells were co-transfected with $Na_V1.2^{WT}$, $Na_V1.2^{\Delta 1897}$, or Nav1.2 $Na_V1.2^{1897\text{-}STOP}$ plasmid (2 μg) with *Scn1b* (2 μg) and EGFP (0.2 μg) and grown in 60-mm culture dishes for 48 hours before recording. Na^+ currents were elicited with a 50 ms depolarization step from -100 mV with 5 mV increment at a holding potential of -120 mV. Steady-state inactivation were tested by a two-pulse protocol with the first pulse of 500 ms from -140 mV to -20 mV at 5 mV increment followed by a second pulse fixed at -20 mV. Gating activation curves were obtained using a Boltzmann function: $G/G_{max} = (1+\exp[-(V-V_{1/2})/k])^{-1}$, where G/G_{max} is the conductance normalized to its maximal value, V is the membrane potential, $V_{1/2}$ is the membrane voltage at which the current amplitude is half-maximal, and *k* is the slope factor. For steady-state inactivation, Na^+ currents induced by the second pulse were normalized to the maximal current and plotted as the function of the voltages elicited by the first pulse, which was also fitted with Boltzmann function: $I/I_{max} = (1+\exp[(V-V_{1/2})/k])^{-1}$, where I/I_{max} is the normalized value. Neuronal Na^+ currents were recorded in pyramidal and non-pyramidal shaped neurons in 5-7 DIV culture at the holding potential of -100 mV. AP was elicited with 5 ms or 500 ms depolarization current in pyramidal shape neurons from 6-9 DIV cultures, and the resting membrane potential was held around -60 mV with current injection.

Brain slice was placed in recording chamber on the stage of an upright, infrared-differential interference contrast microscope (BX51WI, Olympus Optical) equipped with an ORCA-Flash2.8 C11440 Digital CMOS Camera (Hamamatsu Photonics), and was continuously superfused at a rate of 2 ml/min with aCSF bubbled with

95% O2 and 5% CO2 at 35 ± 0.04 °C. mPFC layer 5/6 or BLA pyramidal neurons were visualized with a 40X water-immersion objective. sEPSCs were recorded at -50 mV (near E_{Cl}) and sIPSCs were obtained at 0 mV (near E_{cation}).

Recording pipettes were pulled from borosilicate glass with Sutter P-97 Micropipette Puller (Sutter Instrument Co). Pipette resistance ranged from 1.9 to 2.9 MΩ and 2.9 to 4 MΩ, series resistance was 6.4 ± 0.3 MΩ and 8.6 ± 0.5 MΩ, and compensated by 80% and 60~70%, for Na^+ current recording in HEK cells and neurons, respectively. The pipette resistance ranged from 2.7 to 6.0 MΩ and series resistance was 11.1 ± 0.3 MΩ without compensation for the recordings of post-synaptic currents in brain slices. In current patch-clamp experiments, input resistance was 222 ± 12.7 MΩ for *WT* and 218 ± 20.2 MΩ for *Scn2a*$^{\Delta 1898/+}$. Junction potential was measured immediately after recording by quickly detaching pipette from the recorded cell. The measured junction potential was 2.2 ± 0.3 mV for *WT* and 1.4 ± 0.2 mV for *Scn2a*$^{\Delta 1898/+}$ and data were not corrected.

Behavior analyses. Male and female heterozygous mice and their respective littermates (3-5 months old) were randomly assigned into experimental groups to perform locomotion, elevated plus maze (EPM), three-chamber social interaction, and grooming behavioral tests. Specific protocols for these behavior tests were previously described (45). Male and female *Scn2a*$^{\Delta 1898/+}$ mice were compared to their respective male and female *WT* littermate controls and the investigator analyzing behaviors was blinded to the genotype.

Locomotor activity measurement. The locomotor activity of *WT* and *Scn2a*$^{\Delta 1898/+}$ mice was measured in a 27.3 × 27.3 cm open-field locomotor activity chamber using open-field activity software (MED Associates). Distance traveled during the one-hour test period was evaluated.

Grooming test. Grooming assay was performed in a dimly lit room (~150 lux). Mice were allowed to habituate to the testing room for at least 30 minutes prior to the initiation of the assay. Each mouse was placed into a housing cage with low bedding, and its behaviors were recorded for 30 minutes. A new clean housing cage was used for each mouse. Grooming behavior was auto-scored using pre-trained autoscoring software validated previously (46).

Three-chamber social interaction test. The social test apparatus consisted of a box divided into three chambers of equal size 20 cm (length) x 40.5 cm (width) x 22 cm (height). A testing mouse was introduced to the middle chamber and left to habituate for 5 min followed by another 5 min three-chamber habituation by

removing the retractable walls. After that, the mouse was briefly confined back to the middle chamber, and an unfamiliar mouse (Stranger) was introduced into a wire cage in one of the side-chambers and an object was introduced into a wire cage on the opposite side-chamber. The testing mouse was allowed to freely explore all three chambers for 5 min after removing the retractable walls. All activities of mouse in the chambers were recorded using AnyMaze software (Stoelting Co). Time spent in each chamber and time spent in the contact zone (1.5" zone surrounding the wire cage containing the stranger mouse or object) were collected to evaluate sociability. The location of the stranger mouse and object were alternated between the two side-chambers across the mice tested to avoid a side preference bias. Stranger mice (C57BL/6 male, 3 months old) were purchased from Jackson Laboratories. Prior to behavioral testing, mice were habituated to the behavioral suite on each testing day.

Elevated Plus Maze (EPM) test. The EPM test was performed in an apparatus with two open arm and two closed arms. Two open arms (25 x 5 x 0.5 cm) across each other were perpendicular to 2 closed arms (25 x 5 x 16 cm) with a center platform (5 x 5 x 0.5 cm). The maze was elevated 40 cm above the floor. Experiments started by placing a mouse on the central platform facing an open arm. During the 5 minutes free exploration, the number of entries into each arm, the time spent, and distance traveled in the arm were recorded using AnyMaze software (Stoelting Co.).

Stereotaxic viral delivery and fiber photometry. As previously described (47), the cohort of mice used for the EPM test in conjunction with fiber photometry recording were anesthetized with isoflurane, and 0.2 µl pAAV1-Syn-GCaMP6s-WPRE-SV40 (Addgene, MA) was unilaterally injected into mPFC (AP: +2.00 mm, ML: −0.25 mm, DV: −2.25 mm). During the same surgery, a 400-µm-diameter optical fiber (Doric) was implanted above the injection site in the mPFC (AP: +2.00 mm, ML: −0.25 mm, DV: −2.15 mm) and was secured with Metabond. Animals were tested 3 weeks post-surgery.

Fiber photometry was performed to measure *in vivo* calcium dynamics during EPM. Mice were habituated to the patch cord 1 min in their home cage prior to behavioral testing. During the 5 min test, a 470 nm LED excitation light (M470F3, Thorlabs) delivered at 521 Hz was passed through a filter (FF02-472/30, Semrock), and reflected by a dichroic (FF495-Di03, Semrock) and coupled to the 0.48 NA, 400 µm core optical fiber patch cord (Doric) in order to excite GCAMP6s within neurons. Emitted fluorescence signals traveled back through the patch cord, passed through a dichroic filter (FF01-535/50, Semrock), and was captured by a photodetector (Model 2151,

Newport). The modulated signal was demodulated and low pass filtered using a corner frequency of 15 Hz through a RP2.1 real-time processor (Tucker Davis Technologies). A TTL pulse was sent to the processor at the start of each behavioral trial to allow the alignment of calcium signal recording to mouse behavior. Following behavioral testing, fluorescence microscopy was utilized to confirm GCAMP6s expression and optical fiber placement. Mice with improper placements were eliminated from the analyses.

Data was analyzed using custom MATLAB script. Raw fluorescence signals were first detrended to account for any photobleaching by fitting a third degree polynomial in 15s time windows and subtracting this polynomial from the raw signal trace to calculate ΔF/F. Next, the fluorescent signal was time locked to behavior as defined by entering the open or closed arm. Data was converted to a z-score to account for variability in the dynamic range of the signal across animals and trials, and neural activity was quantified as the mean z-score. To quantify the fluorescence level prior to arm entries during EPM, the mean z-score was calculated over the 1 second prior to every arm entry as determined from behavioral data.

Simons VIP analysis. The Simons VIP v.3.0 data was queried for individuals who had an *SCN2A* variant and also had completed in-person clinical phenotyping. Autism diagnoses were confirmed with the Autism Diagnostic Observation Schedule (ADOS) (27). Caregivers completed the Autism Diagnostic Interview-Revised (ADI-R), a standardized interview that is administered by a trained clinician with research reliability in administration and scoring (26). The ADI-R asks about current and past behaviors. Analyses focused on the Social Disinhibition item and caregiver responses were coded into 4 categories (normal social disinhibition; occasional social disinhibition; definite social disinhibition; marked social disinhibition). Data was analyzed from current behavior only.

Statistics. Numerical averages are presented as mean ± SEM. Unless otherwise stated, statistical significance was calculated using the unpaired *t* test, one way or two-way ANOVA followed by multiple comparisons test, based on the specific data set.

Study Approval. The study was approved by Weill Cornell Medical College Animal Care and Welfare Committee (protocol # 2016-0042).

ACKNOWLEDGMENTS

Supported by NIH T32 DA039080 (C.C.B.); the Leon Levy Foundation and a generous gift from the Mortimer D. Sackler Family Foundation (R.M.J.); NIH R01 NS052819 (F.S.L.); NIH R01 DA029122, The Hartwell Foundation, and the Weill Cornell Autism Research Program (A.M.R); NIH R01 HL112918, R01 HL122967, R01 MH118934, Simons Foundation SFARI Explorer Award # 349984, and Holland-Trice Scholars Award (G.S.P.). We thank Dr. Douglas Kim Laboratory at Janelia Research Campus of HHMI for sharing their pAAV1-Syn-GCaMP6s-WPRE-SV40 virus through Addgene.

Conflict of Interest Statement: The authors have declared that no conflict of interest exists.

Author Contributions: H-GW, FSL, AMR, and GSP designed research studies; H-GW, CCB, AL, and YB conducted experiments; H-GW, CCB, AL, and YB acquired data; H-GW, CCB, AL, JH, RMJ, YB, AMR, and GSP analyzed data; H-GW, AMR, and GSP wrote the manuscript.

REFERENCES

1. Yamagata T, Ogiwara I, Mazaki E, Yanagawa Y, and Yamakawa K. Nav1.2 is expressed in caudal ganglionic eminence-derived disinhibitory interneurons: Mutually exclusive distributions of Nav1.1 and Nav1.2. *Biochem Biophys Res Commun.* 2017;491(4):1070-6.
2. Boiko T, Rasband MN, Levinson SR, Caldwell JH, Mandel G, Trimmer JS, et al. Compact myelin dictates the differential targeting of two sodium channel isoforms in the same axon. *Neuron.* 2001;30(1):91-104.
3. Boiko T, Van Wart A, Caldwell JH, Levinson SR, Trimmer JS, and Matthews G. Functional specialization of the axon initial segment by isoform-specific sodium channel targeting. *J Neurosci.* 2003;23(6):2306-13.
4. Gatto CL, and Broadie K. Genetic controls balancing excitatory and inhibitory synaptogenesis in neurodevelopmental disorder models. *Front Synaptic Neurosci.* 2010;2:4.
5. O'Roak BJ, Vives L, Fu W, Egertson JD, Stanaway IB, Phelps IG, et al. Multiplex targeted sequencing identifies recurrently mutated genes in autism spectrum disorders. *Science.* 2012;338(6114):1619-22.
6. Sanders SJ, Murtha MT, Gupta AR, Murdoch JD, Raubeson MJ, Willsey AJ, et al. De novo mutations revealed by whole-exome sequencing are strongly associated with autism. *Nature.* 2012;485(7397):237-41.
7. Stessman HA, Xiong B, Coe BP, Wang T, Hoekzema K, Fenckova M, et al. Targeted sequencing identifies 91 neurodevelopmental-disorder risk genes with autism and developmental-disability biases. *Nat Genet.* 2017;49(4):515-26.
8. Lim ET, Uddin M, De Rubeis S, Chan Y, Kamumbu AS, Zhang X, et al. Rates, distribution and implications of postzygotic mosaic mutations in autism spectrum disorder. *Nat Neurosci.* 2017;20(9):1217-24.
9. Wolff M, Johannesen KM, Hedrich UBS, Masnada S, Rubboli G, Gardella E, et al. Genetic and phenotypic heterogeneity suggest therapeutic implications in SCN2A-related disorders. *Brain.* 2017;140(5):1316-36.
10. Ben-Shalom R, Keeshen CM, Berrios KN, An JY, Sanders SJ, and Bender KJ. Opposing Effects on NaV1.2 Function Underlie Differences Between SCN2A Variants Observed in Individuals With Autism Spectrum Disorder or Infantile Seizures. *Biol Psychiatry.* 2017;82(3):224-32.
11. Spratt PWE, Ben-Shalom R, Keeshen CM, Burke KJ, Jr., Clarkson RL, Sanders SJ, et al. The Autism-Associated Gene Scn2a Contributes to Dendritic Excitability and Synaptic Function in the Prefrontal Cortex. *Neuron.* 2019;103(4):673-85 e5.
12. Shin W, Kweon H, Kang R, Kim D, Kim K, Kang M, et al. Scn2a Haploinsufficiency in Mice Suppresses Hippocampal Neuronal Excitability, Excitatory Synaptic Drive, and Long-Term Potentiation, and Spatial Learning and Memory. *Frontiers in molecular neuroscience.* 2019;12:145.
13. Middleton SJ, Kneller EM, Chen S, Ogiwara I, Montal M, Yamakawa K, et al. Altered hippocampal replay is associated with memory impairment in mice heterozygous for the Scn2a gene. *Nat Neurosci.* 2018;21(7):996-1003.
14. Tatsukawa T, Raveau M, Ogiwara I, Hattori S, Miyamoto H, Mazaki E, et al. Scn2a haploinsufficient mice display a spectrum of phenotypes affecting anxiety, sociability, memory flexibility and ampakine CX516 rescues their hyperactivity. *Mol Autism.* 2019;10(1):15.
15. Lena I, and Mantegazza M. NaV1.2 haploinsufficiency in Scn2a knock-out mice causes an autistic-like phenotype attenuated with age. *Scientific reports.* 2019;9(1):12886.
16. Nelson SB, and Valakh V. Excitatory/Inhibitory Balance and Circuit Homeostasis in Autism Spectrum Disorders. *Neuron.* 2015;87(4):684-98.
17. Rubenstein JL, and Merzenich MM. Model of autism: increased ratio of excitation/inhibition in key neural systems. *Genes Brain Behav.* 2003;2(5):255-67.
18. Yan H, Wang C, Marx SO, and Pitt GS. Calmodulin limits pathogenic Na+ channel persistent current. *J Gen Physiol.* 2017;149(2):277-93.
19. Gade AR, Marx SO, and Pitt GS. An interaction between the III-IV linker and CTD in NaV1.5 confers regulation of inactivation by CaM and FHF. *J Gen Physiol.* 2020;152(2).
20. Planells-Cases R, Caprini M, Zhang J, Rockenstein EM, Rivera RR, Murre C, et al. Neuronal death and perinatal lethality in voltage-gated sodium channel alpha(II)-deficient mice. *Biophys J.* 2000;78(6):2878-91.

21. Ogiwara I, Miyamoto H, Tatsukawa T, Yamagata T, Nakayama T, Atapour N, et al. Nav1.2 haplodeficiency in excitatory neurons causes absence-like seizures in mice. *Communications Biology.* 2018;1(1):96.
22. Silverman JL, Yang M, Lord C, and Crawley JN. Behavioural phenotyping assays for mouse models of autism. *Nat Rev Neurosci.* 2010;11(7):490-502.
23. Moy SS, Nadler JJ, Perez A, Barbaro RP, Johns JM, Magnuson TR, et al. Sociability and preference for social novelty in five inbred strains: an approach to assess autistic-like behavior in mice. *Genes Brain Behav.* 2004;3(5):287-302.
24. Yang M, Silverman JL, and Crawley JN. Automated three-chambered social approach task for mice. *Current protocols in neuroscience.* 2011;Chapter 8:Unit 8.26.
25. Sanders SJ, Campbell AJ, Cottrell JR, Moller RS, Wagner FF, Auldridge AL, et al. Progress in Understanding and Treating SCN2A-Mediated Disorders. *Trends Neurosci.* 2018;41(7):442-56.
26. Rutter M, LeCouteur A, and Lord C. *Autism Diagnostic Interview-Revised (ADI-R) manual.* Los Angeles: Western Psychological Services; 2003.
27. Lord C, Risi S, Lambrecht L, Cook EH, Jr., Leventhal BL, DiLavore PC, et al. The autism diagnostic observation schedule-generic: a standard measure of social and communication deficits associated with the spectrum of autism. *J Autism Dev Disord.* 2000;30(3):205-23.
28. Korenberg JR, Chen XN, Hirota H, Lai Z, Bellugi U, Burian D, et al. VI. Genome structure and cognitive map of Williams syndrome. *J Cogn Neurosci.* 2000;12 Suppl 1:89-107.
29. Sakurai T, Dorr NP, Takahashi N, McInnes LA, Elder GA, and Buxbaum JD. Haploinsufficiency of Gtf2i, a gene deleted in Williams Syndrome, leads to increases in social interactions. *Autism Res.* 2011;4(1):28-39.
30. Barak B, and Feng G. Neurobiology of social behavior abnormalities in autism and Williams syndrome. *Nat Neurosci.* 2016;19(6):647-55.
31. Cryan JF, and Holmes A. The ascent of mouse: advances in modelling human depression and anxiety. *Nat Rev Drug Discov.* 2005;4(9):775-90.
32. Vertes RP. Interactions among the medial prefrontal cortex, hippocampus and midline thalamus in emotional and cognitive processing in the rat. *Neuroscience.* 2006;142(1):1-20.
33. Duvarci S, and Pare D. Amygdala microcircuits controlling learned fear. *Neuron.* 2014;82(5):966-80.
34. Bloodgood DW, Sugam JA, Holmes A, and Kash TL. Fear extinction requires infralimbic cortex projections to the basolateral amygdala. *Transl Psychiatry.* 2018;8(1):60.
35. Luchkina NV, and Bolshakov VY. Mechanisms of fear learning and extinction: synaptic plasticity-fear memory connection. *Psychopharmacology (Berl).* 2019;236(1):163-82.
36. Deneault E, White SH, Rodrigues DC, Ross PJ, Faheem M, Zaslavsky K, et al. Complete Disruption of Autism-Susceptibility Genes by Gene Editing Predominantly Reduces Functional Connectivity of Isogenic Human Neurons. *Stem Cell Reports.* 2018;11(5):1211-25.
37. Feyder M, Karlsson RM, Mathur P, Lyman M, Bock R, Momenan R, et al. Association of mouse Dlg4 (PSD-95) gene deletion and human DLG4 gene variation with phenotypes relevant to autism spectrum disorders and Williams' syndrome. *Am J Psychiatry.* 2010;167(12):1508-17.
38. Chen R, Gore F, Nguyen QA, Ramakrishnan C, Patel S, Kim SH, et al. Deep brain optogenetics without intracranial surgery. *Nat Biotechnol.* 2021;39(2):161-4.
39. Li HH, Roy M, Kuscuoglu U, Spencer CM, Halm B, Harrison KC, et al. Induced chromosome deletions cause hypersociability and other features of Williams-Beuren syndrome in mice. *EMBO Mol Med.* 2009;1(1):50-65.
40. Segura-Puimedon M, Sahun I, Velot E, Dubus P, Borralleras C, Rodrigues AJ, et al. Heterozygous deletion of the Williams-Beuren syndrome critical interval in mice recapitulates most features of the human disorder. *Hum Mol Genet.* 2014;23(24):6481-94.
41. Meyer-Lindenberg A, Hariri AR, Munoz KE, Mervis CB, Mattay VS, Morris CA, et al. Neural correlates of genetically abnormal social cognition in Williams syndrome. *Nat Neurosci.* 2005;8(8):991-3.
42. Cho JH, Deisseroth K, and Bolshakov VY. Synaptic encoding of fear extinction in mPFC-amygdala circuits. *Neuron.* 2013;80(6):1491-507.
43. Hubner C, Bosch D, Gall A, Luthi A, and Ehrlich I. Ex vivo dissection of optogenetically activated mPFC and hippocampal inputs to neurons in the basolateral amygdala: implications for fear and emotional memory. *Front Behav Neurosci.* 2014;8:64.

44. Turrigiano G. Too many cooks? Intrinsic and synaptic homeostatic mechanisms in cortical circuit refinement. *Annu Rev Neurosci.* 2011;34:89-103.
45. Kabir ZD, Che A, Fischer DK, Rice RC, Rizzo BK, Byrne M, et al. Rescue of impaired sociability and anxiety-like behavior in adult cacna1c-deficient mice by pharmacologically targeting eIF2alpha. *Mol Psychiatry.* 2017;22(8):1096-109.
46. Jhuang H, Garrote E, Mutch J, Yu X, Khilnani V, Poggio T, et al. Automated home-cage behavioural phenotyping of mice. *Nature communications.* 2010;1:68.
47. Bavley CC, Fetcho RN, Burgdorf CE, Walsh AP, Fischer DK, Hall BS, et al. Cocaine- and stress-primed reinstatement of drug-associated memories elicit differential behavioral and frontostriatal circuit activity patterns via recruitment of L-type Ca(2+) channels. *Mol Psychiatry.* 2019.

Table 1. Action Potential Induced with Minimum Intensity of 5 ms Depolarization Step

	RMP (mV)	AMP (mV)	TH (mV)	AP50 (ms)	RT (ms)	RS (mV/ms)	DT (ms)	DS (mV/ms)	*N*
WT	-63 ± 0.9	96 ± 2.1	-38 ± 1.2	2.5 ± 0.1	7.0 ± 0.4	8.2 ± 0.5	6.5 ± 1.0	21.5 ± 2.5	29
***Scn2a*$^{\Delta 1898/+}$**	-64 ± 0.5	82 ± 3.0*	-34 ± 0.7*	3.4 ± 0.3*	7.3 ± 0.2	6.9 ± 0.4	10.6 ± 1.6	11.1 ± 2.2*	26

RMP, resting membrane potential; AMP, amplitude; TH, threshold, AP50, half width; RT, 10-100% rise time; RS, 10-100% rise slope; DT, 100-10% decrease time; DS, 100-10% decrease slope. *N*, number. *: *WT* vs *Scn2a*$^{\Delta 1898/+}$, $p < 0.05$ (Multiple *t* tests corrected for multiple comparisons using the Holm-Sidak method).

Table 2. Action Potential with Maximal Amplitude by 5 ms Depolarization Step

	AMP (mV)	TH (mV)	AP50 (ms)	RT (ms)	RS (mV/ms)	DT (ms)	DS (mV/ms)	*N*
WT	111 ± 2.6	-25 ± 1.5	2.2 ± 0.1	4.2 ± 0.1	20.3 ± 0.9	5.1 ± 0.7	29.9 ± 4.0	29
***Scn2a*$^{\Delta 1898/+}$**	105 ± 2.8	-19 ±1.5*	2.6 ± 0.2	4.3 ± 0.1	17.8 ± 0.5	6.8 ± 0.9	17.5 ± 2.3	26

AMP, amplitude; TH, threshold, AP50, half width; RT, 10-100% rise time; RS, 10-100% rise slope; DT, 100-10% decrease time; DS, 100-10% decrease slope. *N*, number. *: *WT* vs *Scn2a*$^{\Delta 1898/+}$, $p < 0.05$ (Multiple *t* tests corrected for multiple comparisons using the Holm-Sidak method).

Figure 1

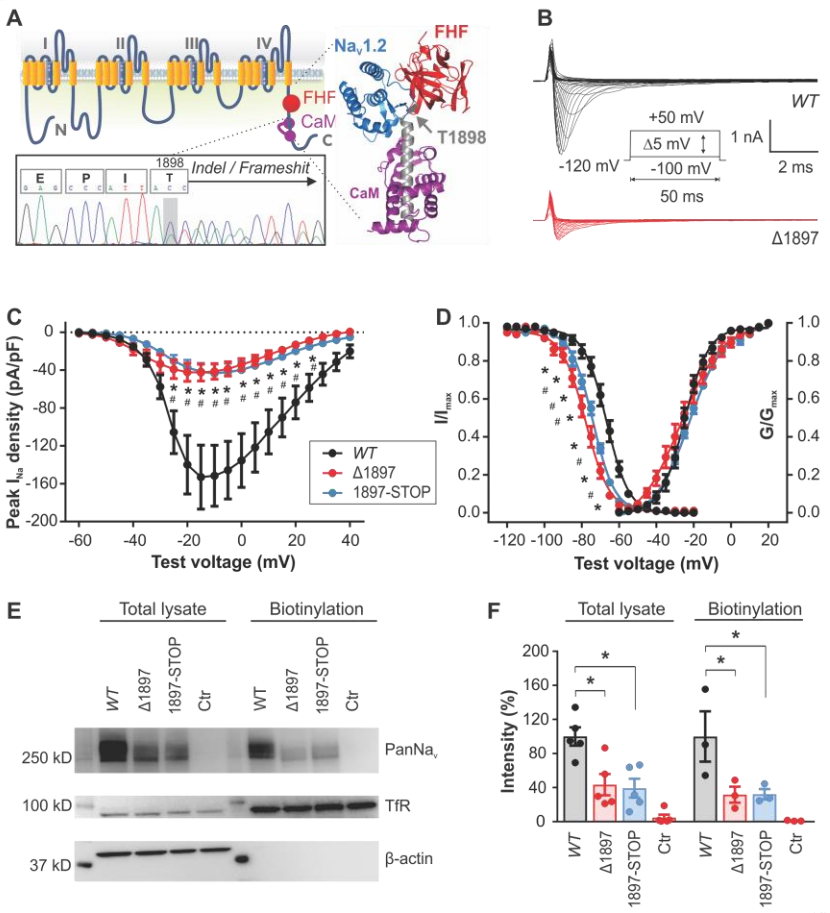

Figure 1. Na$_V$1.2$^{\Delta 1897}$ channels display reduced peak Na$^+$ current density in transfected cells. ***A***, Schematic of the Na$_V$1.2 pore-forming α subunit. The bottom inset showing genomic DNA sequencing, which demonstrates the T1898N frameshift in one of the alleles in *Scn2a*$^{\Delta 1898/+}$ mice. The right inset shows the location of T1898 on the crystal structure (PDB: 4JPZ) of the ternary complex of the Na$_V$1.2 CTD (blue; truncated helix shown in gray), FGF13 (FHF, red), and calmodulin (purple). The arrow indicates the location of T1898. ***B***, Exemplar current traces for Na$_V$1.2^{WT} and the frameshifted/truncated Na$_V$1.2$^{\Delta 1897}$ channel (p. T1897NsfX27, equivalent to T1898 in mice) expressed in HEK293 cells. ***C***, Peak current density-voltage relationships for Na$_V$1.2^{WT} (n=11), Na$_V$1.2$^{\Delta 1897}$ ("Δ1897", n=11) and a Na$_V$1.2 with a stop codon inserted at T1897 ("1897-STOP", n=12). *, two-way ANOVA followed by Dunnett's multiple comparisons test. Peak I_{Na} density*mutation, F (40, 620)=9.732, p<0.0001. ***D***, Steady-state inactivation (I/Imax) (*WT*, n=15; Δ1897, n=11; 1897-STOP, n=12) and activation (G/Gmax) relationships for the three channels. *, two-way ANOVA followed by Dunnett's multiple comparisons test. I/I_{max}*mutation, F (40, 700)=12.34, p<0.0001. ***E***, Exemplar immunoblot of whole cell lysates or the biotinylated surface fraction from HEK293 cells expressing the three channels. Transferrin receptor (TfR) and actin represent a membrane and cytoplasmic marker, respectively, that demonstrate successful separation of the biotinylated membrane fraction. Molecular weight markers are shown on the left. ***F***, Quantification of intensities (relative to *WT*) from immunoblots (total lysate, n=5; biotinylation, n=3). *, one-way ANOVA followed by Dunnett's multiple comparisons test. Total lysate, F (3, 16)=15.4, p<0.0001; Na$_V$1.2^{WT} vs. Na$_V$1.2$^{\Delta 1897}$, p=0.0029; Na$_V$1.2^{WT} vs. 1897-STOP, p=0.0016. Biotinylation, F (3, 8)=6.963, p=0.01; Na$_V$1.2^{WT} vs. Δ1897, p=0.04; Na$_V$1.2^{WT} vs. 1897-STOP, p=0.04.

Figure 2

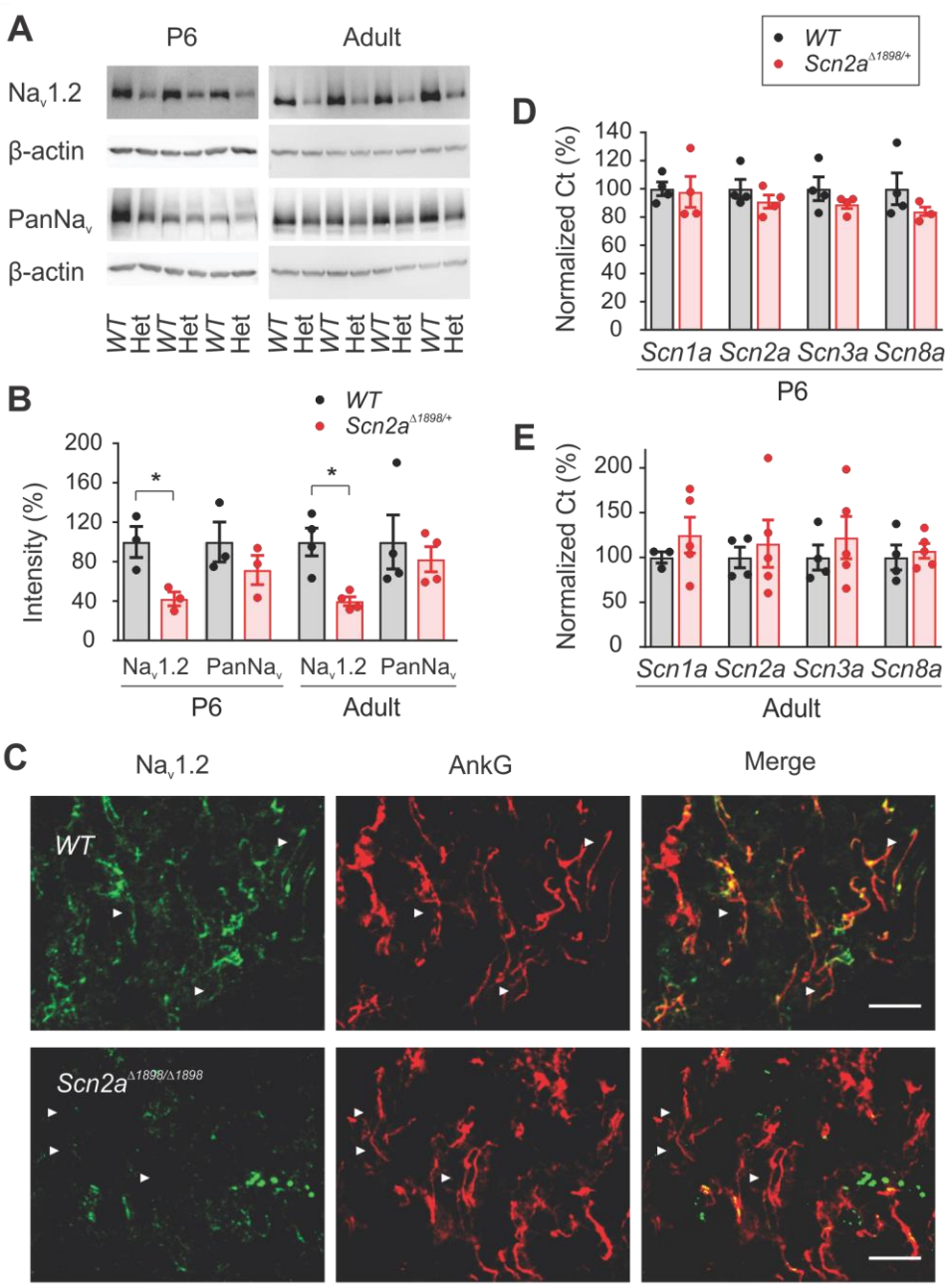

Figure 2. Cortices from *Scn2a*$^{\Delta 1898/+}$ mice have less total and Na$_V$1.2 voltage-gated Na$^+$ channels. ***A***, Immunoblots for Na$_V$1.2 (anti-Nav1.2, recognizes amino acids 1882-2005) or total voltage-gated Na$^+$ channel (PanNa$_V$) in brain cortex lysates from P6 (n=3) or adult (~5 month, n=4) *WT* or *Scn2a*$^{\Delta 1898/+}$ (Het) mice. Molecular weights are shown on the left. β-actin serves as a loading control and for normalization in ***B***, which shows the quantification of Na$_V$1.2 and total Na$^+$ channels as in panel ***A***, normalized to *WT*. *: unpaired *t* test, t (4)=3.348, *p*=0.03 for P6; t (6)=4.07, *p*=0.007 for adult. ***C***, Immunohistochemistry of layer 2/3 in cortex from P0.5 mice stained with anti-Nav1.2 and anti-ankyrin G (AnkG) antibodies. The arrows indicate axonal Nav1.2 or AnkG. Scale bar, 10 μm. ***D and E*****,** Relative (normalized to GAPDH) CNS Na$^+$ channel transcripts quantified by RT-qPCR in P3-6 (n=4) and adult (~5 month; *WT*, n=4; *Scn2a*$^{\Delta 1898/+}$, n=5) cortex, respectively.

Figure 3

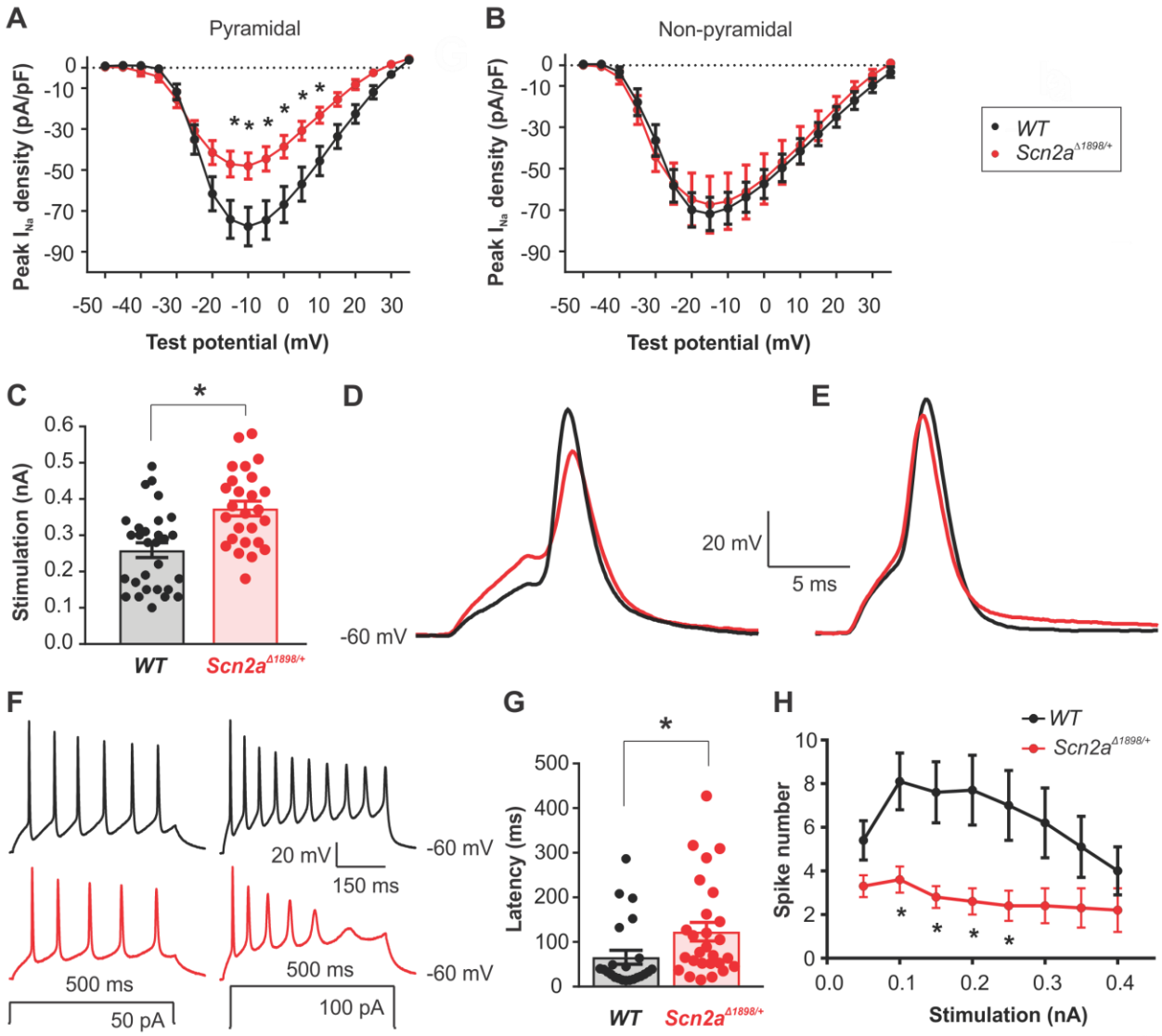

Figure 3. Cortical neurons from *Scn2a*$^{\Delta 1898/+}$ mice display reduced voltage-gated Na^+ channel current and reduced excitability. ***A***, Current-voltage relationship for excitatory (pyramidal) neurons (*WT*, n=14; *Scn2a*$^{\Delta 1898/+}$, n=17). *, two-way ANOVA followed by Sidak's multiple comparisons test. Peak I_{Na} density*genotype, F (16, 464)=6.73, p<0.0001. ***B***, Current-voltage relationship for inhibitory (non-pyramidal) neurons (*WT*, n=12; *Scn2a*$^{\Delta 1898/+}$, n=12). ***C***, Stimulation threshold to elicit action potentials in cultured cortical neurons isolated from *WT* (n=29) or *Scn2a*$^{\Delta 1898/+}$ (n=26) *: unpaired t-test, t(53)=3.961, p=0.0002. ***D***, Exemplar action potentials from *WT* or *Scn2a*$^{\Delta 1898/+}$ elicited at threshold stimulation. ***E***, Exemplar action potentials from *WT* or *Scn2a*$^{\Delta 1898/+}$ elicited at a stimulation intensity (0.4±0.03 nA and 0.6±0.02 nA, for *WT* and *Scn2a*$^{\Delta 1898/+}$, respectively) that elicits the maximal amplitude. ***F***, Exemplar evoked action potential trains elicited from *WT* (n=23) or *Scn2a*$^{\Delta 1898/+}$ (n=27) with 500 ms current injection of 50 pA or 100 pA. The resting membrane potential is indicated (bottom right). ***G***, Latency of first spike at minimum stimulation intensity, *: unpaired t-test, t(48)=2.135, p=0.038. ***H*,** The number of evoked action potentials for the indicated intensity of current injection. *, two-way ANOVA followed by Sidak's multiple comparisons test. Spike number*genotype, F (11, 528)=6.693, p<0.0001.

Figure 4

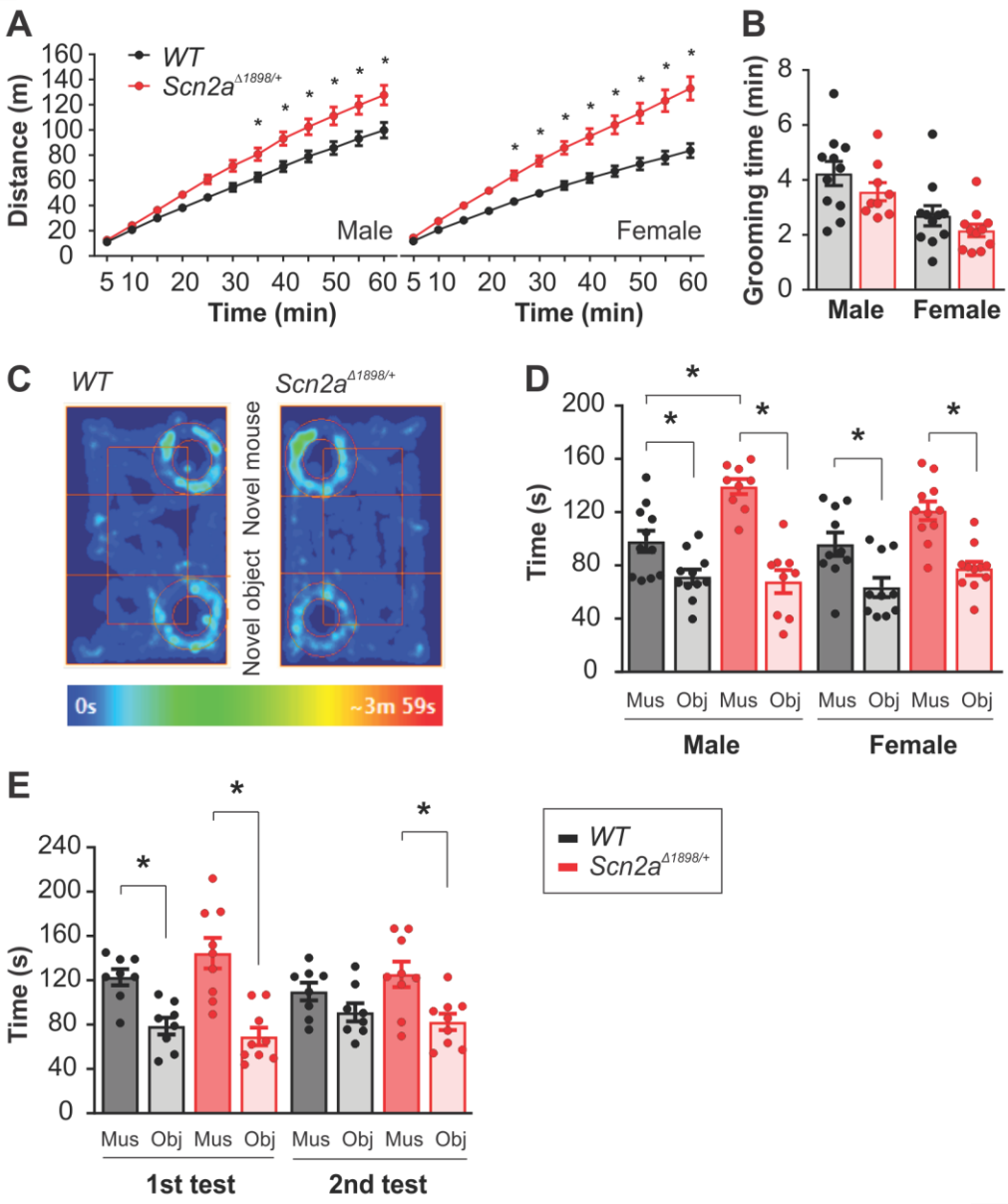

Figure 4. *Scn2a*$^{\Delta 1898/+}$ mice display hyperactivity in a novel environment and show increased social interactions. ***A***, Hyperactivity in *Scn2a*$^{\Delta 1898/+}$ male and female mice compared to *WT* littermate controls in an open field (male: *WT*, n=11 and *Scn2a*$^{\Delta 1898/+}$, n=9; female: *WT*, n=11 and *Scn2a*$^{\Delta 1898/+}$, n=11). *, two-way ANOVA followed by Sidak's multiple comparisons test. Distance*genotype, F (11, 198)=8.278 for male and F (11, 220)=16.27 for female, $p<0.0001$. ***B***, Grooming time. ***C***, Heat maps from three chamber social interaction tests for *WT* (male, n=11; female, n=10) and *Scn2a*$^{\Delta 1898/+}$ (male, n=9; female, n=11) mice. ***D***, Time spent with novel mouse (Mus) or novel object (Obj) in the three-chamber social interaction test. *, two-way ANOVA followed by Turkey's multiple comparisons test. Mus or Obj*genotype, F (1, 36)=9.963, $p=0.003$ for male; F (1, 38)=0.5996, $p=0.445$ for female. Mus vs Obj Turkey's multiple comparisons test, *WT*, $p=0.04$; *Scn2a*$^{\Delta 1898/+}$ $p<0.0001$ for male; *WT*, $p=0.02$, *Scn2a*$^{\Delta 1898/+}$ $p=0.0004$ for female. ***E,*** Repeated three three-chamber social interaction tests in a separate cohort of male *WT* (n=8) and *Scn2a*$^{\Delta 1898/+}$ (n=9) mice. Unpaired *t* test was used to evaluate the difference in time spent between Mus and Obj. Both *WT* (t (14)=4.174, $p=0.0009$) and *Scn2a*$^{\Delta 1898/+}$ (t (16)=4.721, $p=0.0002$) mice spent more time with novel Mus over Obj during the 1st test, but only *Scn2a*$^{\Delta 1898/+}$ mice displayed a social preference 3 hours later (2nd test) to the familiar Mus (t (16)=3.149, $p=0.0062$).

Figure 5

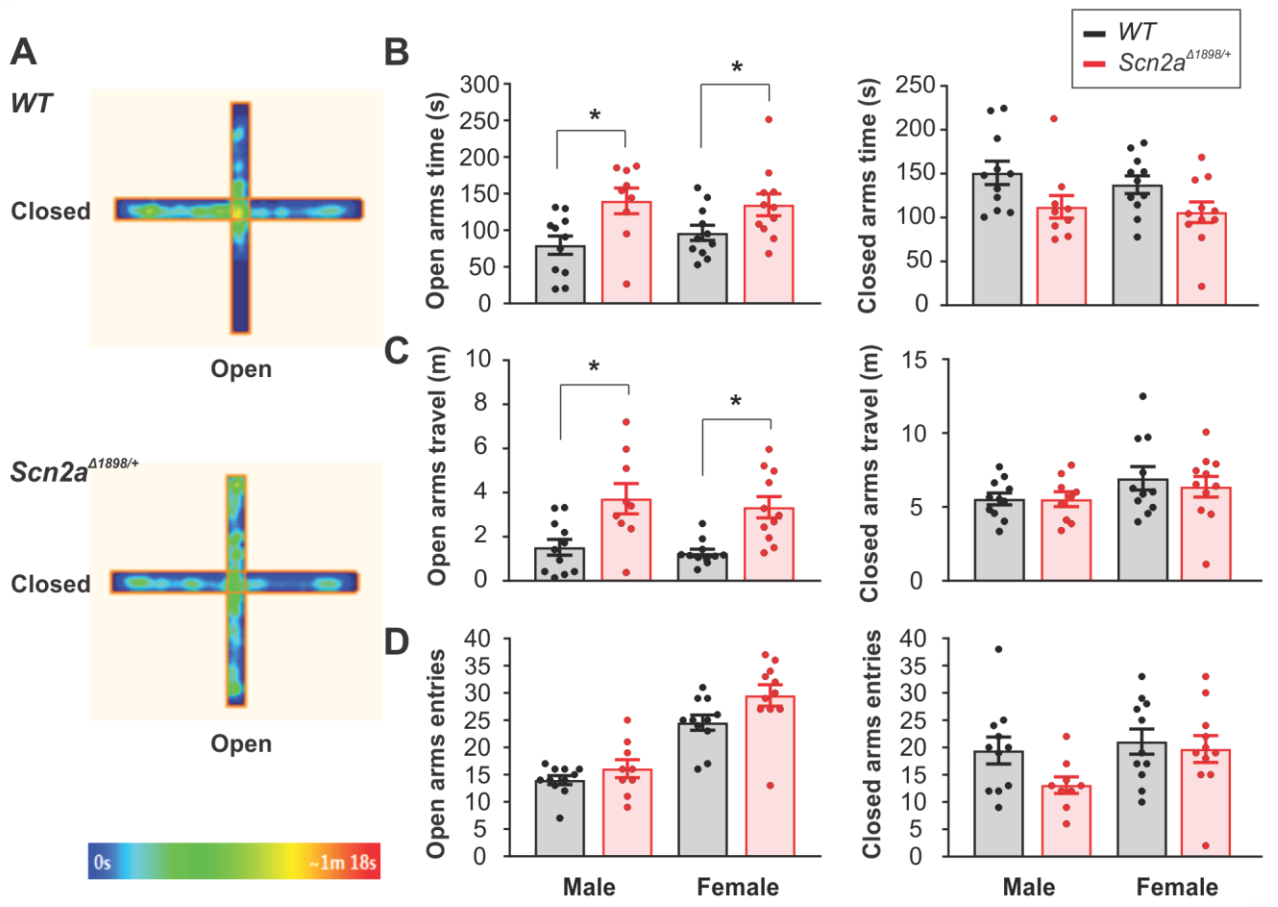

Figure 5. *Scn2a*$^{\Delta 1898/+}$ mice display increased time and travelled distance on the EPM open arms. ***A***, Exemplar heat maps for *WT* (male, n=11; female, n=11) and *Scn2a*$^{\Delta 1898/+}$ (male, n=9; female, n=11) on the EPM. ***B***, Time spent in the open and closed arms. *, unpaired *t* test, t (18)=2.886, *p*=0.01 for male; t (20)=2.103, *p*=0.048 for female. ***C***, Distance traveled in the open and closed arms. *: unpaired *t* test, t (18)=2.998, *p*=0.008 for male; t (20)=4.07, *p*=0.001 for female. ***D***, Number of entries to the open and closed arms.

Figure 6

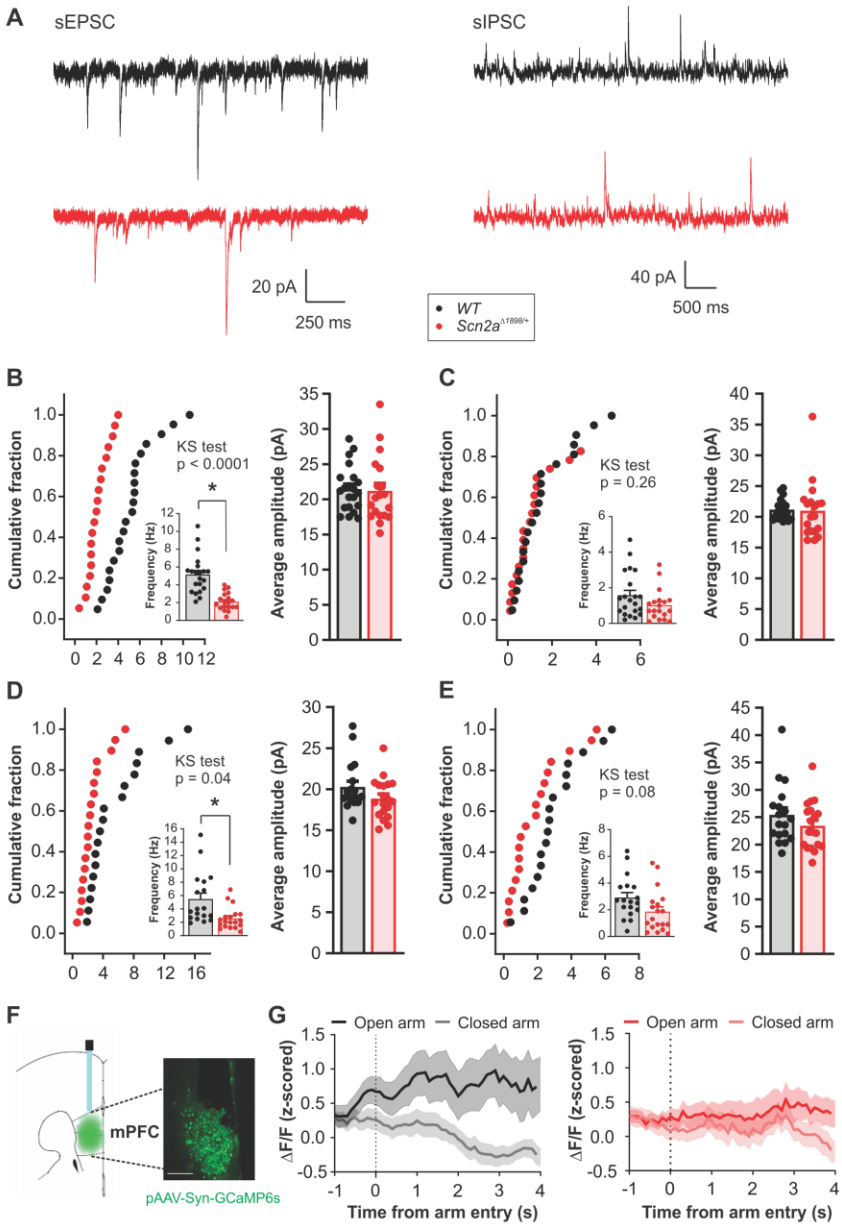

Figure 6. Pyramidal neurons in mPFC and BLA from *Scn2a*$^{\Delta 1898/+}$ mice display altered excitability and synaptic properties. ***A***, Exemplar sEPSCs and sIPSCs recorded in pyramidal neurons from *Scn2a*$^{\Delta 1898/+}$ and *WT* mice at holding potential of -50 mV and 0 mV, respectively. *WT*, colored in black; *Scn2a*$^{\Delta 1898/+}$, colored in red. ***B, C***, Quantification of frequency and amplitude of sEPSCs and sIEPSCs (*Scn2a*$^{\Delta 1898/+}$, n=19; *WT*, n=21) recorded in layer 5/6 pyramidal neurons in mPFC. Frequency of sEPSCs reduced as shown in both cumulative fraction and average (inset, *, unpaired *t* test, t (38)=5.691, $p<0.0001$). ***D, E***, Quantification of frequency and amplitude of sEPSCs and sIEPSCs (*Scn2a*$^{\Delta 1898/+}$, n=19; *WT*, n=18) recorded in pyramidal neurons in BLA. Frequency of sEPSCs reduced as shown in both cumulative fraction and average (inset, *, unpaired *t* test, t (35)=3.027, $p=0.005$). The cumulative frequency distributions were analyzed with the Kolmogorov-Smirnov Comparison (KS test) in ***B-E***. ***F***, Microscopic graph showing the GCaMP6s virus expression and fiber placement in mPFC. ***G,*** Calcium dynamics in GCaMP6s-expressed neurons with fiber photometry recording during EPM. In contrast to *WT* mice, *Scn2a*$^{\Delta 1898/+}$ mice failed to show an increase in fluorescent [Ca^{2+}] signal when mice entered the open arms compared with the closed arms.